THE JOURNAL OF BIOLOGICAL CHEMISTRY VOL. 282, NO. 35, pp. 25801–25816, August 31, 2007

Modulation of Androgen Receptor Activation Function 2 by Testosterone and Dihydrotestosterone*

Received for publication, April 18, 2007, and in revised form, June 25, 2007 Published, JBC Papers in Press, June 25, 2007, DOI 10.1074/jbc.M703268200

Emily B. Askew[‡§], **Robert T. Gampe, Jr.**[¶], **Thomas B. Stanley**[¶], **Jonathan L. Faggart**[§‖], **and Elizabeth M. Wilson**[‡§‖**‡‡1]

From the [‡]*Curriculum in Toxicology,* [§]*Laboratories for Reproductive Biology,* [**]*Lineberger Comprehensive Cancer Center, and the Departments of* [‖]*Pediatrics and* [‡‡]*Biochemistry and Biophysics, University of North Carolina, Chapel Hill, North Carolina 27599 and* [¶]*Computational and Structural Sciences, Division of Molecular Discovery Research, GlaxoSmithKline, Research Triangle Park, North Carolina 27709*

The androgen receptor (AR) is transcriptionally activated by high affinity binding of testosterone (T) or its 5α-reduced metabolite, dihydrotestosterone (DHT), a more potent androgen required for male reproductive tract development. The molecular basis for the weaker activity of T was investigated by determining T-bound ligand binding domain crystal structures of wild-type AR and a prostate cancer somatic mutant complexed with the AR F*XX*LF or coactivator L*XX*LL peptide. Nearly identical interactions of T and DHT in the AR ligand binding pocket correlate with similar rates of dissociation from an AR fragment containing the ligand binding domain. However, T induces weaker AR F*XX*LF and coactivator L*XX*LL motif interactions at activation function 2 (AF2). Less effective F*XX*LF motif binding to AF2 accounts for faster T dissociation from full-length AR. T can nevertheless acquire DHT-like activity through an AR helix-10 H874Y prostate cancer mutation. The Tyr-874 mutant side chain mediates a new hydrogen bonding scheme from exterior helix-10 to backbone protein core helix-4 residue Tyr-739 to rescue T-induced AR activity by improving AF2 binding of F*XX*LF and L*XX*LL motifs. Greater AR AF2 activity by improved core helix interactions is supported by the effects of melanoma antigen gene protein-11, an AR coregulator that binds the AR F*XX*LF motif and targets AF2 for activation. We conclude that T is a weaker androgen than DHT because of less favorable T-dependent AR F*XX*LF and coactivator L*XX*LL motif interactions at AF2.

The androgen receptor (AR)[2] is a member of the nuclear receptor superfamily of ligand-activated transcription factors. Androgen activation of AR regulates prostate growth, bone and muscle mass, and spermatogenesis and is a predisposing factor in prostate cancer. AR mediates transcriptional activity in response to two biologically active androgens that bind AR with similar high affinity (1). Testosterone (T) is the major circulating androgen secreted by the testis and the active androgen in muscle. Dihydrotestosterone (DHT), the 5α-reduced metabolite of T, is a more potent androgen required for male reproductive tract development.

AR has a modular structure composed of an NH_2-terminal transactivation domain, central DNA binding domain, linker hinge region, and carboxyl-terminal ligand binding domain (LBD) (2). Like other nuclear receptor family members (3), AR has two major activation domains. Androgen-induced AR transcriptional activity depends on activation function 1 in the largely unstructured NH_2-terminal region (2) and activation function 2 (AF2), a highly ordered hydrophobic surface in the LBD that requires androgen binding for its structural integrity (4).

The degree to which AF2 contributes to overall AR activity depends on multiple competing factors. Unlike other nuclear receptors, AR AF2 binds a number of L*XX*LL-related motifs. Important among these is the AR NH_2-terminal F*XX*LF motif ^{23}FQNLF^{27} that binds AF2 in an androgen-dependent and -specific manner. AR F*XX*LF motif binding to AF2 is the basis for the AR NH_2- and carboxyl-terminal (N/C) interaction (5–7) that contributes to AR dimerization (8, 9) and is critical for AR regulation of androgen-dependent genes (10–12). The functional significance of the AR N/C interaction *in vivo* is supported by the effects of several naturally occurring mutations that disrupt AR F*XX*LF motif binding and cause resistance to androgen without diminishing high affinity androgen binding (13–16). The androgen insensitivity syndrome results in varying degrees of incomplete masculinization of the external gen-

* This work was supported by United States Public Health Service Grant NICHD HD16910 from the National Institutes of Health, NICHD Grant U54-HD35041 of the specialized Cooperative Centers Program in Reproductive Research of the National Institutes of Health, NCI Grant P01-CA77739 from the National Institutes of Health, and by Grant T32 ES007126 from the Curriculum in Toxicology, University of North Carolina, Chapel Hill. The costs of publication of this article were defrayed in part by the payment of page charges. This article must therefore be hereby marked "*advertisement*" in accordance with 18 U.S.C. Section 1734 solely to indicate this fact.

The atomic coordinates and structure factors (code 2q7I, 2q7J, 2Q7K, 2Q7L) have been deposited in the Protein Data Bank, Research Collaboratory for Structural Bioinformatics, Rutgers University, New Brunswick, NJ (http://www.rcsb.org/).

[1] To whom correspondence should be addressed: Laboratories for Reproductive Biology, CB 7500, University of North Carolina, Chapel Hill, NC 27599-7500. Tel.: 919-966-5168; Fax: 919-966-2203; E-mail: emw@med.unc.edu.

[2] The abbreviations used are: AR, androgen receptor; T, testosterone; DHT, dihydrotestosterone; LBD, ligand binding domain; AF2, activation function 2; N/C, NH_2- and carboxyl-terminal; SRC, steroid receptor coactivator; MAGE-11, melanoma antigen gene protein-11; WT, wild-type; TIF2, transcriptional intermediary factor 2; H-bond, hydrogen bond; PSA, prostate-specific antigen; MMTV, mouse mammary tumor virus; PBS, phosphate-buffered saline; R1881, 17α-methyltrienolone; androstanediol, 5α-androstane-3α,17β-diol; ERβ, estrogen receptor-β; E_2, estradiol; androstenedione, 4-androstene-3,17-dione; r.m.s.d., root mean squared difference; Bistris propane, 1,3-bis[tris(hydroxymethyl)methylamino]propane.

italia in genetic males depending on the extent to which the mutation disrupts AR function (17).

In addition to the AR F*XX*LF motif, multiple related motifs bind the AR AF2 site with relatively high affinity (18). F*XX*LF motifs are present in a number of putative AR coregulatory proteins and interact at AF2 (19, 20). Within the AR NH_2-terminal domain is a W*XX*LF motif that interacts with the AR AF2 site in the presence of androgen but with weaker affinity than the AR F*XX*LF motif (5, 10). Similar to other nuclear receptors, AR AF2 serves as the binding site for steroid receptor coactivator (SRC)/p160 coactivator L*XX*LL motifs. Crystal structures demonstrate overlapping binding sites for AR F*XX*LF and coactivator L*XX*LL motifs (4, 18). Based on peptide display screening (18, 20, 21) and binding affinity measurements (4), AR AF2 preferentially binds F*XX*LF motifs compared with coactivator L*XX*LL motifs. In addition, we have shown that androgen-dependent AR F*XX*LF motif binding to AF2 in the AR N/C interaction competitively inhibits coactivator L*XX*LL motif binding (19).

The contribution of AF2 to AR transcriptional activity is also influenced by cell- and tissue-specific coactivators, some of which selectively increase accessibility of AF2 to coactivator recruitment. One mechanism proposed to increase AR AF2 activity in prostate cancer is higher levels of SRC/p160 coactivators that compete for the AR N/C interaction and increase AR transcriptional activity through AF2 (10, 22). The AR coregulator melanoma antigen gene protein-11 (MAGE-11) of the MAGEA gene family binds the AR F*XX*LF motif to expose AF2 and increase coactivator recruitment (23). Naturally occurring AR somatic mutations in prostate cancer can increase AR activity by enhancing SRC/p160 coactivator recruitment to AF2 (7). The relative binding affinities and competitive relationships at the AF2 site suggest that high affinity androgen binding triggers sequential interactions of multiple coregulatory proteins.

In this study we provide biochemical and structural evidence that T is a less effective androgen than DHT because of weaker T-dependent F*XX*LF and L*XX*LL motif binding at the AR AF2 surface. This conclusion is supported by a prostate cancer somatic mutation AR-H874Y that increases the transcriptional response to T in association with improved F*XX*LF and L*XX*LL motif binding at AF2. Crystal structure determination of T-bound WT and H874Y AR LBD provided some insight into the possible differential molecular effects of T *versus* DHT. Receptor bound with T appears to induce isolated conformational heterogeneity at the AF2 surface. The AR H874Y mutation creates new direct hydrogen (H) bonds between core helix residues that probably contribute to the molecular basis for the described functional rescue by this prostate cancer mutant.

EXPERIMENTAL PROCEDURES

Plasmids—pCMVhAR vectors expressing full-length human AR with H874Y, E897K, and K720A mutations (6, 14, 24) and AR-(507–919) which lacks the NH_2-terminal region (2) were described. Coding sequences for AR-(663–919) and AR-(663–919)-H874Y were inserted at the NdeI and BamHI sites of the pET-15b bacterial expression vector by PCR amplification of corresponding pCMVhAR mutant plasmids. GAL-AR-(658–919) and H874Y, E897K, and K720A mutants were created by PCR amplification of respective pCMVhAR plasmids and subcloning into Tth111I- and XbaI-digested pGAL0. GAL-AR-(640–919) was created by PCR amplifying the fragment from pCMVhAR and subcloning into NdeI- and XbaI-digested pGAL0. VP-AR-(1–660) (13), VP-TIF2-(624–1287) (VP-TIF2.1) (25), GAL-AR-(624–919), and H874Y, E897K, and K720A mutants (7), prostate-specific antigen-enhancer-luciferase (PSA-Enh-Luc) (26), mouse mammary tumor virus (MMTV)-Luc, 5XGAL4Luc3 (10), and pSG5-MAGE-11 coding for full-length MAGE-11 residues 1–429 (23) were described. All PCR-amplified regions were verified by DNA sequencing.

Reporter Gene Assays—The CWR-R1 prostate cancer cell line derived from the CWR22 recurrent human prostate cancer xenograft (24, 27) was plated at 1.6 or 2×10^5 cells/well in 12-well plates in prostate cell growth medium containing Richter's improved minimal essential medium (Invitrogen) or Dulbecco's modified Eagle's medium (Invitrogen) supplemented with 5 ng/ml selenium, 10 mM nicotinamide, 5 μg/ml insulin, 5 μg/ml transferrin, and 2% fetal bovine serum and transfected using Effectene (Qiagen). Endogenous CWR-R1 cell AR-H874Y transcriptional activity was detected using 0.1 μg/well MMTV-Luc reporter vector. AR AF2 activity was determined in CWR-R1 cells by transfecting 0.1 μg of WT or mutant GAL-AR-(624–919) or GAL-AR-(658–919) and 0.25 μg of 5XGAL4Luc3. For two-hybrid interaction assays, CWR-R1 cells were transfected with 50 ng of VP-TIF2-(624–1287), WT, or mutant GAL-AR-(624–919) and 0.1 μg of 5XGAL4Luc3. For 12-well plates, DNA was combined with (per well) 45 μl of transfection buffer (Qiagen) and 1 μl of Enhancer, vortexed, and incubated for 5 min at room temperature. Effectene (1 μl/well) was added, vortexed for 10 s, and incubated for 10 min at room temperature. Prostate cell growth medium (0.2 ml) was added and vortexed, and 220 μl of DNA solution was added to each well containing 1 ml of medium. The next day cells were washed with phosphate-buffered saline (PBS) and 1 ml of phenol red-free, serum-free basic prostate medium containing Improved minimal essential Zinc Option medium (Invitrogen), and the indicated steroids were added per well. Cells were incubated at 37 °C overnight, washed with PBS, and harvested in 0.25 ml of lysis buffer containing 1% Triton X-100, 2 mM EDTA, and 25 mM Tris phosphate, pH 7.8. Cells were rocked at room temperature for 30 min in lysis buffer, and 0.1 ml of cell lysate was analyzed for luciferase activity using a Lumistar Galaxy (BMG Labtech) automated multiwell plate reader luminometer.

Human epithelial cervical carcinoma HeLa cells were maintained in Eagle's minimum essential medium supplemented with 10% fetal bovine serum (Gemini or HyClone), penicillin, streptomycin, and 2 mM L-glutamine. For reporter gene assays, HeLa cells were plated at 5×10^4 cells/well in 12-well plates and 24 h later transfected using FuGENE 6 transfection reagent (Roche Applied Science) with 10 ng of pCMVhAR or H874Y mutant and 0.25 μg of PSA-Enh-Luc reporter vector to determine androgen-induced AR transactivation. To measure AR AF2 activity, HeLa cells were transfected with 0.1 μg of GAL-AR-(658–919) and the H874Y mutant and 0.25 μg of 5XGAL4Luc3. For two-hybrid interaction assays, HeLa cells

were transfected with 0.1 μg of 5XGAL4Luc3, 50 ng of VP-AR-(1–660) or VP-TIF2-(624–1287), and 50 ng of GAL-AR-(624–919), -(640–919), -(658–919), or GAL-AR-(624–919)-H874Y. DNA was added to 43 μl of serum-free medium and 0.6 μl of FuGENE-6 reagent per well. After a 15-min incubation, 40 μl of FuGENE/DNA mixture was added to each well containing 1 ml of medium. The next day cells were washed with PBS, and 1 ml/well serum-free medium lacking phenol red containing the indicated steroids was added and incubated overnight at 37 °C. Twenty four hours later cells were washed with PBS and assayed for luciferase activity after harvesting in 0.25 ml of lysis buffer as described above.

Monkey kidney CV1 cells were maintained in Dulbecco's modified Eagle's medium containing 10% bovine calf serum (HyClone), 2 mM L-glutamine, penicillin, streptomycin, and 20 mM HEPES, pH 7.2. Cells (4.2×10^5/6 cm dish) were plated in medium containing 5% bovine calf serum and 24 h later transfected using calcium phosphate DNA precipitation (28). The effect of TIF2 on AR AF2 activity was determined by transfecting 5 μg of 5XGAL4Luc3 and 0.1 μg of GAL-AR-(624–919), GAL-AR-(658–919), or the H874Y mutants in the absence and presence of 2 μg of pSG5-TIF2. The effect of MAGE-11 on AR transcriptional activity was determined by transfecting 0.1 μg of pCMVhAR or pCMVhAR-H874Y and 5 μg of PSA-Enh-Luc in the absence and presence of 2 μg of pSG5-MAGE-11 and 2 μg of pSG5-TIF2. Cells were incubated overnight with and without the indicated androgens and the next day placed in serum-free medium in the absence and presence of androgen. After 24 h cells were washed with PBS, harvested in 0.25 ml of lysis buffer, and assayed for luciferase activity as described.

Immunoblots—Relative expression levels of WT and mutant GAL-AR-(624–919), GAL-AR-(658–919), pCMVhAR, and pCMVhAR-(507–919) were determined by immunoblot analysis. COS-1 cells were plated at 2×10^6 cells/10-cm dish in 10% bovine calf serum (HyClone) in Dulbecco's modified Eagle's medium containing penicillin, streptomycin, 2 mM L-glutamine, and 20 mM HEPES, pH 7.2, and transfected using DEAE-dextran (28). After 24 h, medium containing 1 μM MG132 (Sigma), a proteosome inhibitor, was added to cells expressing GAL-AR-(624–919) and GAL-AR-(658–919) and readded after an overnight incubation and incubated for 1 h. Cells were washed with 8 ml of cold PBS, harvested in 1 ml of PBS, and solubilized in 0.1 ml of RIPA buffer containing 1% Nonidet P-40, 0.5% sodium deoxycholate, 0.1% SDS, 1 mM dithiothreitol, 1 mM phenylmethylsulfonyl fluoride, and complete protease inhibitor mixture (Roche Applied Science). Protein concentrations were determined using the Bio-Rad assay with bovine serum albumin as standard. Protein extracts were separated on a 10% acrylamide gel containing SDS and analyzed by immunoblot. GAL4 fusion proteins were detected using rabbit polyclonal anti-GAL antibody (Santa Cruz Biotechnology) at 1:500 dilution. AR was detected using rabbit polyclonal AR52 immunoglobulin G (29) at 2 μg/ml. Incubations with primary antibody were for 1 h at room temperature. Anti-rabbit horseradish peroxidase-conjugated secondary IgG antibody (Amersham Biosciences) was used at 1:10,000 dilution for 1 h at room temperature. Signals were detected using chemiluminescence (SuperSignal West Dura Extended Duration Substrate, Pierce).

Androgen Dissociation Rate Assays—Ligand dissociation rate studies were performed at 37 °C in whole cell binding assays by plating 4×10^5 COS cells/well of 6-well plates and transfecting 1 or 2 μg of pCMVhAR, pCMVhAR-(507–919), or H874Y mutant per well using DEAE-dextran (28). Transfected cells were incubated for 2 h at 37 °C in 0.6 ml of serum-free medium lacking phenol red and containing 5 nM [1,2,6,7-^{3}H]T (78.5 Ci/mmol) or 3 nM [1,2,4,5,6,7-^{3}H]DHT (124 Ci/mmol). Nonspecific binding was determined in parallel wells by adding 100-fold molar excess of unlabeled androgen. Timed dissociation rates were determined by amending to 50 μM T or 17α-methyltrienolone (R1881) (PerkinElmer Life Sciences) to the labeling media added in 0.1 ml of medium. Cultured cell incubations at 37 °C were terminated at different times, and cells were washed with PBS, harvested in 0.5 ml of lysis buffer containing 2% SDS, 10% glycerol, and 20 mM Tris, pH 6.8, and radioactivity was determined by scintillation counting. Dissociation half-times were determined as the mean ± S.E. time required to reduce specific androgen binding by 50%.

Protein Preparation—Crystallography grade AR LBD (human AR residues 663–919) and AR-H874Y LBD with an NH_2-terminal His_6 tag and thrombin cleavage site were expressed from pET-15b in BL-21 DE3 *Escherichia coli*. Cells were grown overnight at 18 °C in 2× YT bacterial growth medium (16 g/liter tryptone-B, 10 g/liter yeast extract-B, 5 g/liter $NaCl_2$, Bio 101 Systems, Q-Biogene) containing 0.1 g/liter carbenicillin (Sigma), 1 mM isopropyl thiogalactopyranoside, and 0.5 mM T added from a 347 mM stock in dimethyl sulfoxide. Cells resuspended in urea extraction buffer (50 ml of 25 mM Tris, pH 8.0, 0.3 M $NaCl_2$, and 2 M urea per 10 g of cells) were lysed with an APV LAB 1000 homogenizer and centrifuged at 40,000 rpm for 45 min at 4 °C. The supernatant was loaded onto a Ni^{2+}-charged immobilized nickel metal affinity-Sepharose column (ProBond, Invitrogen) equilibrated with 25 mM Tris, pH 8.0, 0.3 M $NaCl_2$, and 50 mM imidazole. A linear gradient to 1 M imidazole with 25 mM Tris, pH 8.0, and 0.3 M $NaCl_2$ was used to elute the AR LBD. Pooled fractions were amended with thrombin (5 NIH units/mg protein; Sigma) and NaCl to ~0.4 M and dialyzed (15,000 molecular weight cutoff, Spectra/Por membrane) overnight at 4 °C against a buffer containing 10 μM T, 25 mM Tris, pH 8.0, 0.4 M $NaCl_2$, 5 mM DTT, 2 mM EDTA, and 10% glycerol. The digested AR LBD was diluted 8-fold with 25 mM HEPES, pH 7.5, 50 mM $NaCl_2$, 5 mM DTT, 2 mM EDTA, and 10% glycerol and immediately loaded onto a 5-ml HiTrap SP-HP-Sepharose ion exchange column, washed with dilution buffer, and eluted using a linear gradient to 1 M $NaCl_2$ with 25 mM HEPES, pH 7.5, 5 mM DTT, 2 mM EDTA, and 10% glycerol. Samples containing AR LBD were combined, amended to 10 μM T and 0.5 M $NaCl_2$, and concentrated with a Centriprep centrifugal filter unit (Amicon) to <10 ml. Size exclusion chromatography was performed on the concentrated pooled ion exchange chromatography purified fractions using a HiLoad Superdex S75 (26/60) size exclusion column (GE Healthcare). Purified AR LBD was eluted with buffer containing 10 μM T, 25 mM HEPES, pH 7.5, 0.15 M $LiSO_4$, 10 mM DTT, 0.5 mM EDTA, and 10% glycerol and concentrated to 2–4 mg/ml using a Centriprep centrifugal filter unit. The final sample buffer contained

10 μM T, 25 mM HEPES, pH 7.5, 0.15 M Li_2SO_4, 10 mM DTT, 0.5 mM EDTA, 10% glycerol, and 0.05% β-*n*-octoglucoside.

Fluorescence Polarization Measurements of Peptide Binding Affinity—Fluorescence binding studies were performed using WT AR LBD and AR-H874Y LBD expressed in *E. coli* in the presence of 0.5 mM T or 50 μM DHT. Protein was purified as described above except AR LBD-DHT thrombin digestion and overnight dialysis were not performed, and DHT was not readded during purification. Protein was concentrated to 0.6–3 mg/ml using Centriprep centrifugal filter units in buffer containing 10 μM T or DHT, 0.15 M Li_2SO_4,10 mM DTT, 0.5 mM EDTA, 10% glycerol, 0.05% β-*n*-octoglucoside, and 25 mM HEPES, pH 7.5. AR F*XX*LF and TIF2 L*XX*LL peptide binding affinities were determined by fluorescence polarization at room temperature for 1 h using 5–40 μM AR LBD and AR-H874Y LBD purified in the presence of 10 μM ligand and assayed with

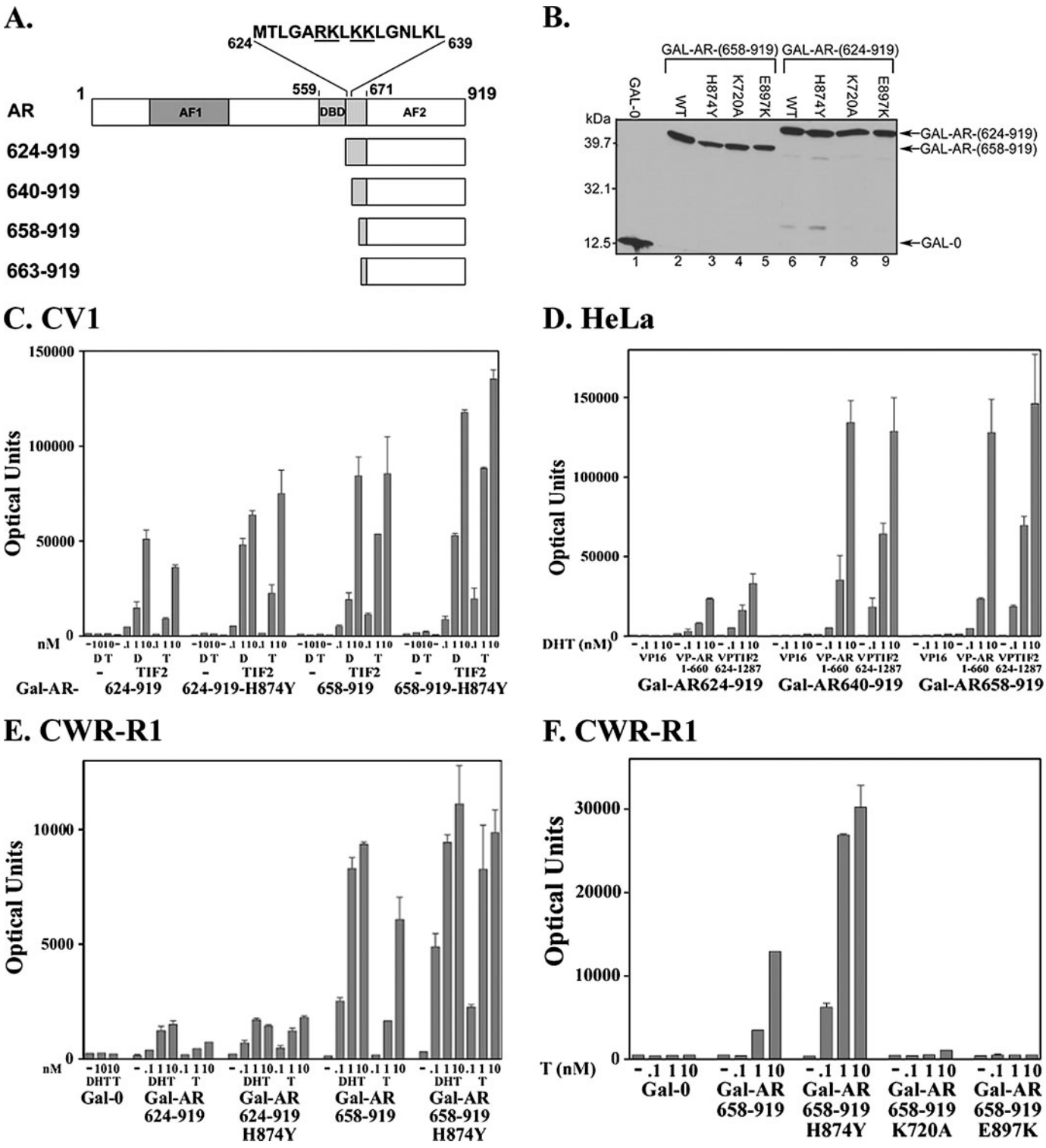

and without addition to 40 μM DHT or T and 10 nM AR-(20–30) fluorescein-RGAFQNLFQSV or TIF2 third L*XX*LL motif 732–756 fluorescein-QEPVSPKKKENALLRYLLDKDDTKD (Synpep, Dublin, CA). As a control, human estrogen receptor-β (ERβ) LBD (residues 257–530) was analyzed in parallel in the presence of 40 μM estradiol (E_2). Fluorescence polarization values were determined using an Envision (PerkinElmer Life Sciences) fluorescence plate reader with 485 nm excitation and 520 nm emission filters. Binding isotherms were constructed, and K_D values were determined by nonlinear least squares fit based on a 1:1 interaction (30).

Crystallization and Data Analysis—Concentrated solutions of purified AR-H874Y LBD and AR LBD complexed with T and amended with 2–3 M excess of AR-(20–30) F*XX*LF motif peptide RGAFQNLFQSV or TIF2-(740–753) L*XX*LL-III motif peptide KENALLRYLLDKDD were used to obtain diffraction grade crystals. Vapor diffused hanging drops at 22 °C with a 1:1 (v/v) ratio of the AR complex and the precipitant solution produced ~150–200 μm crystals within 3–15 days. Salt solutions containing 0.6 M sodium-potassium tartrate and Bistris propane, pH 7.0, or Tris, pH 8.5, were used as precipitants. Prior to flash-freezing in liquid N_2, crystals were transiently mixed with a cryoprotectant solvent consisting of precipitant solution amended to 20% glycerol. X-ray diffraction data were collected at 100 K with an ADSC 210 detector at the IMCA-CAT, sector 17ID, or a MAR225 CCD detector at the SER-CAT, sector 22BM, at the Advanced Photon Source synchrotron. Diffraction data were integrated and scaled with HKL2000 (31).

Structure Determination and Refinement—An initial model for the T-bound AR-H874Y LBD with AR-(20–30) peptide data was determined by molecular replacement with MolRep (32, 33) and the AR LBD coordinates from the AR-DHT structure (34) (Protein Data Bank access code 1I37). The convincing solution contained a single AR LBD complex in the asymmetric unit that had excellent quality 1.8 Å resolution electron density for T and the respective peptide. Multiple cycles of manual model building with COOT (35) and maximum likelihood restrained refinement with all hydrogens were performed with Refmac (36) in all cases. Initial models for the remaining data sets were determined and refined in a similar manner. Table 3 summarizes the crystallographic and refinement statistics. Coordinate files with hydrogens were generated with MolProbity (37). To eliminate possible slight differences arising from variation in AF2 helix position, backbone heavy atoms for AR chain A LBD residues 680–890 were used for structure superimposition and performed with the CCP4i LSQAB utility using coordinates without hydrogens. Reported interatomic distances are between heavy atoms unless specified, and the angles with protons when necessary were measured with COOT or PyMol. Structure figures were generated with PyMol from Delano Scientific.

RESULTS

AF2 Activation by T and DHT—To investigate the differential effects of T and DHT on AR AF2 activity, we performed studies using WT AR and a prostate cancer somatic mutant AR-H874Y that has an increased transcriptional response to T (7, 24). To optimize detection of AR AF2 activity, we varied the length of the hinge region of several AR LBD-GAL4-DNA binding domain fusion proteins expressed in several cell lines (Fig. 1*A*). In CV1 cells, T and DHT increased TIF2-dependent GAL-AR-(658–919) activity to a greater extent than GAL-AR-(624–919), indicating inhibition by hinge residues that include the AR nuclear targeting signal (38) (Fig. 1*C*). The H874Y mutation increased androgen sensitivity and overall transcriptional activity but remained dependent on ligand and coexpression of TIF2 (Fig. 1*C*).

Transcriptional activity of GAL-AR-(624–919), -(640–919), and -(658–919) was also low in HeLa cells without coexpression of TIF2 (Fig. 1*D*). In two-hybrid assays, GAL-AR-(640–919) and GAL-AR-(658–919) interacted to a greater extent than GAL-AR-(624–919) with VP-AR-(1–660) indicative of the AR N/C interaction and with VP-TIF2-(624–1287) reflecting coactivator L*XX*LL motif binding to AF2 (Fig. 1*D*) (4–8).

Androgen-dependent AF2 activity of GAL-AR-(658–919) was stronger in the CWR-R1 prostate cancer cell line and was detected independent of coexpressed TIF2 (Fig. 1*E*). Activity of GAL-AR-(658–919) was greater than GAL-AR-(624–919), and the H874Y mutation increased the response to T. Differences in transcriptional activity did not result from differences in protein expression (Fig. 1*B*) and was AF2-dependent because

FIGURE 1. **AF2 activity in the AR LBD.** *A,* schematic diagram of AR LBD deletion mutants. Full-length human AR (amino acid residues 1–919) contains activation function 1 (AF1, amino acid residues 142–337), DNA binding domain (DBD residues 559–623), hinge region residues 624–670, and LBD residues 671–919 that includes AF2. AR hinge region residues 624–639 contain the carboxyl-terminal portion of the bipartite AR nuclear targeting signal residues Arg-629, Lys-630, Lys-632, and Lys-633 (*underlined*) (38). AR-(624–919), -(640–919), and -(658–919) with WT and mutant sequence were expressed as GAL4 DNA binding domain fusion proteins. AR residues 663–919 and H874Y mutant were expressed for crystallography as His_6-tagged fusion proteins with intervening thrombin cleavage site. *B,* similar expression of GAL-AR-LBD fusion proteins. COS cells were transfected with 10 μg of GAL-0 (*lane 1*), GAL-AR-(658–919) (*lanes 2–5*), and GAL-AR-(624–919) (*lanes 6–9*) with WT or mutant sequence. Protein extracts (60 μg of protein/lane) were separated on a 10% acrylamide gel containing SDS and the blot probed using an anti-GAL antibody. *C,* androgen-dependent activity of GAL-AR-(624–919), GAL-AR-(658–919) WT and H874Y mutants in CV1 cells requires coexpression of TIF2. CV1 cells plated in 6-cm dishes were transfected by calcium phosphate DNA precipitation with 5 μg of 5XGAL4Luc3 reporter vector and 0.1 μg of GAL-AR-(624–919) or GAL-AR-(658–919) with WT or H874Y sequence in the absence and presence of 2 μg of pSG5-TIF2. Cells were treated with and without increasing concentrations of DHT (*D*) and T as indicated and luciferase activity was determined. Data are representative of three independent experiments. *D,* inhibition of the AR N/C and coactivator interactions by AR hinge residues 624–639. HeLa cells were transfected using FuGENE 6 by adding per well 0.1 μg of 5XGAL4Luc, 50 ng of VP16, VP-AR-(1–660), or VP-TIF2-(624–1287) with 0.1 μg of GAL-AR-(624–919), -(640–919), or -(658–919). Cells were incubated with and without 0.1–10 nM DHT for 24 h as indicated and assayed for luciferase activity. Data are representative of three independent experiments. *E,* androgen-dependent transcriptional activity of GAL-AR-(624–919), GAL-AR-(658–919), and H874Y mutants in CWR-R1 cells. CWR-R1 cells (2×10^5/well) were transfected using Effectene by adding per well 0.1 μg of GAL-AR-(624–919), GAL-AR-(658–919), or H874Y mutants and 0.25 μg of 5XGAL4Luc3. Cells were treated with and without increasing concentrations of T and DHT for 24 h as indicated, and luciferase activity was determined. Data are representative of three independent experiments. *F,* androgen-dependent AF2 activity of GAL-AR-(658–919) in CWR-R1 cells. CWR-R1 cells (2×10^5/well) were transfected using Effectene by adding per well 0.1 μg of GAL-AR-(658–919) or H874Y, K720A, or E897K mutants and 0.25 μg of 5XGAL4Luc3. Lys-720 and Glu-897 are charge clamp residues in AF2. Cells were incubated with and without 0.1, 1, and 10 nM T for 24 h, and luciferase activity was determined. Data are representative of at least three independent experiments.

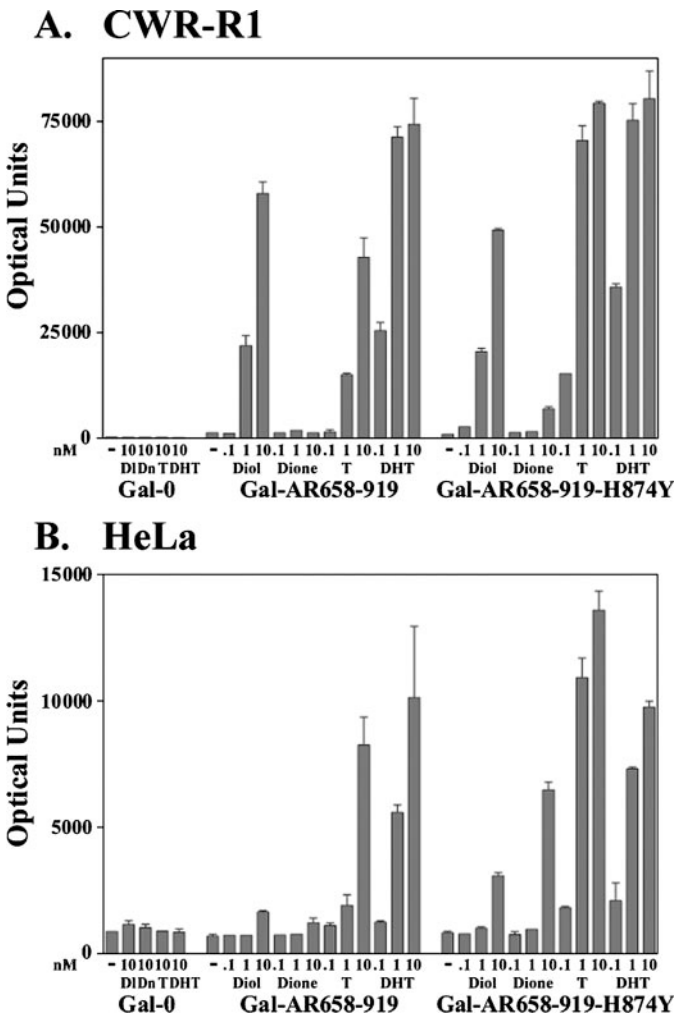

FIGURE 2. **Increased AR-H874Y LBD AF2 activity response to T.** *A,* CWR-R1 prostate cancer cells (2×10^5/well) were transfected using Effectene by adding per well 0.1 μg of GAL-0, GAL-AR-(658–919), or H874Y mutant and 0.25 μg of 5XGAL4Luc3. Cells were incubated in the absence and presence of 0.1, 1, and 10 nM 5α-androstane-3α,17β-diol (*DI, Diol*), androstenedione (*Dn, Dione*), T and DHT for 24 h as indicated, and luciferase activity was determined. *B,* HeLa cells were transfected using FuGENE 6 by adding per well 0.1 μg of GAL-0, GAL-AR-(658–919), or H874Y mutant and 0.25 μg of 5XGAL4Luc3. Transfected cells were incubated with and without androgen as indicated for 24 h and assayed for luciferase activity. Data in *A* and *B* are representative of at least three independent experiments.

charge clamp mutants K720A and E897K eliminated the response (Fig. 1*F*).

Thus, differential effects of T and DHT on WT and H874Y AR AF2 activity were evident in CWR-R1 cells using GAL-AR-(658–919), which avoided the inhibitory effects of AR hinge residues ^{624}MTLGARKLKKLGNLKL^{639} (39) (AR nuclear targeting signal underlined) (38).

Increased AR-H874Y AF2 Activation by T and Adrenal Androgens—The magnitude and dose response of GAL-AR-(658–919)-H874Y AF2 activity by T in CWR-R1 cells were similar to DHT but less than the WT with T (Figs. 1*E* and 2*A*). GAL-AR-(658–919)-H874Y activity was also greater with 4-androstene-3,17-dione compared with WT. Androstanediol activated WT and H874Y GAL-AR-(658–919) equivalent to WT with T.

In HeLa cells, the predominant effect of the H874Y mutation was also increased sensitivity to T (Fig. 2*B*), whereas GAL-AR-(658–919) and the H874Y mutant responded similarly to DHT. We noted a lack of transcriptional response by GAL-AR-(658–919) to androstanediol in HeLa cells, which contrasted equivalent activity by androstanediol and T in CWR-R1 cells. Two-hybrid studies suggested that the greater activity by androstanediol in CWR-R1 cells resulted from metabolism to an active androgen (data not shown).

Full-length endogenous AR-H874Y in CWR-R1 cells does not activate the PSA-Luc reporter (40) but activates MMTV-luciferase in response to T and DHT and higher concentrations of androstenedione and androstanediol (Fig. 3*A*). Transiently expressed AR and AR-H874Y in CWR-R1 cells activate PSA-Luc in response to T and DHT, and adrenal androgens were more effective with AR-H874Y (data now shown). In HeLa cells, AR-H874Y lacked constitutive activity but increased the response to T with less differential effects by DHT, androstenedione, and androstanediol (Fig. 3*B*).

The results in both CWR-R1 and HeLa cell lines suggest that the predominant effect of the H874Y mutation is to increase the AF2 response to T. Our ability to detect AR AF2 activity in CWR-R1 cells but not HeLa or CV1 cells without coexpression of TIF2 likely reflects higher endogenous SRC/p160 coactivator levels in CWR-R1 cells that endogenously express the AR-H874Y mutant (40).

Preferential AF2 Activation by MAGE-11—MAGE-11 is an AR coregulator expressed in prostate cancer cell lines and in normal tissues of the human male and female reproductive tracts (23). MAGE-11 binds the AR NH_2-terminal F*XX*LF motif and increases AF2 by inhibiting the AR N/C interaction. To gain further evidence that AR-H874Y increases AF2 activity in response to T, we determined the effect of MAGE-11 with and without coexpression of TIF2 using a PSA-luciferase reporter.

Coexpression of TIF2 had minimal effects on AR and AR-H874Y activity (Fig. 4) in agreement with the inhibitory effects of the AR N/C interaction on coactivator recruitment by AF2 (28). Coexpression of MAGE-11 with and without TIF2 preferentially increased AR-H874Y activity in response to T compared with WT AR and AR-H874Y with DHT. AR-H874Y activity induced by T and DHT was nearly equal in the presence of MAGE-11 with or without TIF2. This contrasts WT AR where DHT induced greater activity than T in the presence of MAGE-11 with or without TIF2. Coexpression of MAGE-11 also increased ligand independent activity of AR-H874Y more than WT AR. Differences in transcriptional activity were independent of differences in protein expression levels based on immunoblot analysis (see Fig. 6*B*). The preferential effects of MAGE-11 on T-dependent AR-H874Y activity suggest that H874Y imparts DHT-like activity to T by increasing coactivator recruitment to AF2.

FXXLF and LXXLL Motif Binding Affinities—Binding isotherms calculated by fluorescence polarization indicate WT AR LBD-DHT binds the AR F*XX*LF peptide with ~2-fold higher affinity than WT AR LBD–T with no significant change by the H874Y mutation (Fig. 5; Table 1). Similar results were observed for the TIF2 L*XX*LL peptide except overall binding affinities were weaker than the F*XX*LF peptide. ERβ LBD-E_2 bound the TIF2 L*XX*LL peptide with higher affinity than the F*XX*LF peptide as reported previously (4). The data suggest a direct differ-

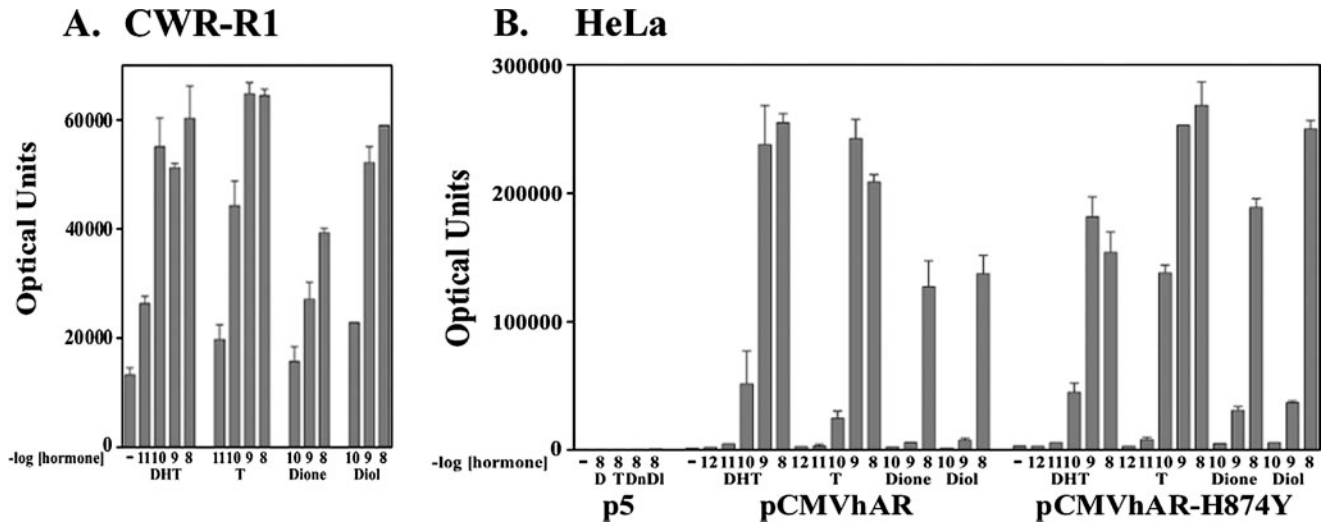

FIGURE 3. **Increased transcriptional activity of AR-H874Y by T and adrenal androgens.** *A,* CWR-R1 cells (1.6×10^5 cells/well) were transfected with 0.1 μg of MMTV-Luc/well of 12-well plates using Effectene. Cells were incubated in the absence and presence of increasing concentrations of DHT, T, androstenedione (*Dione*), and androstanediol (*Diol*) as indicated for 24 h and assayed for luciferase activity. *B,* HeLa cells were transfected using FuGENE 6 by adding per well 10 ng of pCMV5 empty vector (p5), pCMVhAR, or the H874Y mutant and 0.25 μg of PSA-Enh-Luc. Cells were incubated with and without 0.001 to 10 nM DHT (*D*) or T, and 0.1 to 10 nM androstenedione (*Dn, Dione*) or 5α-androstane-3α,17β-diol (*DI, Diol*) for 24 h before luciferase activity was determined. Data in *A* and *B* are representative of three independent experiments.

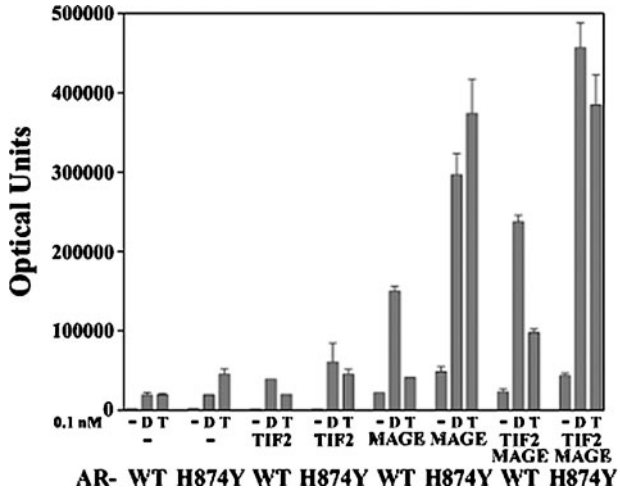

FIGURE 4. **MAGE-11 increases AR-H874Y activity response to T and DHT.** CV1 cells plated in 6-cm dishes were transfected using calcium phosphate DNA precipitation by adding per dish 0.1 μg of WT pCMVhAR (AR-WT) or H874Y mutant and 5 μg of PSA-Enh-Luc reporter in the absence and presence of 2 μg of pSG5-TIF2 and/or 2 μg of pSG5-MAGE-11–(1-429) (*MAGE*) as indicated. Cells were incubated with and without 0.1 nM T for 48 h before luciferase activity was determined. Data are representative of three independent experiments.

ential effect of T and DHT on AF2 motif binding affinity that is not altered by the H874Y mutation.

T and DHT Dissociation Kinetics—Prostate cancer mutation H874Y slows the dissociation rate of synthetic androgen R1881 from AR and AR-(507–919), a carboxyl-terminal fragment that lacks the AR NH_2-terminal domain (7). To investigate the similar AR-H874Y AF2 activity induced by T and DHT, we determined androgen dissociation half-times from WT and H874Y full-length AR and AR-(507–919) containing the DNA binding domain and LBD, which expressed similarly on immunoblots (Fig. 6*B*).

T dissociates 3–4 times faster than DHT from full-length WT AR (Fig. 6*A*; Table 2) (1) but with a similar rate as DHT from AR-(507–919) (Table 2), suggesting similar steroid contacts in the ligand binding pocket. T dissociates 3–4 times slower from AR-H874Y than from WT AR at a rate similar to DHT dissociation from AR and AR-H874Y. The dissociation rate of T and DHT from AR-(507–919)-H874Y was ~2-fold slower than from WT AR-(507–919).

The data indicate that slow dissociation of DHT from full-length WT AR results predominantly from interactions outside the ligand binding pocket, and H874Y has effects inside and outside the binding pocket. The similar half-time of T dissociation from AR-H874Y to DHT from AR and AR-H874Y parallel AF2 transcriptional activities (see Figs. 1 and 2) and provide further evidence that H874Y imparts DHT-like activity to T by increasing the transcriptional activity of AF2.

T-bound WT AR LBD and AR-H874Y LBD Structures—We determined the crystal structures of WT and H874Y AR LBD bound with T in the presence of the AR-(20–30) NH_2-terminal F*XX*LF motif peptide or TIF2 coactivator peptide TIF2-(740–753) third L*XX*LL motif. Crystallographic refinement data are provided in Table 3. Globally, all four structures conform to the canonical nuclear receptor LBD fold (Fig. 7, *A* and *B*) and when superimposed are nearly identical based on r.m.s.d. statistics for the *xyz* displacement relative to the WT AR LBD–T-F*XX*LF coordinates (0.26 Å for WT AR LBD-T-L*XX*LL, 0.14 Å for AR-H874Y LBD–T-F*XX*LF, and 0.27 Å for AR-H874Y LBD-T-L*XX*LL). Globally, the structures concur with previously reported structures for WT AR LBD bound to DHT and R1881 and prostate cancer mutants AR-T877A LBD and AR-W741L LBD bound to steroid and nonsteroid ligands (4, 18, 34, 41–45). Our WT AR LBD-T structures with AR F*XX*LF (Protein Data Bank access code 2Q7I) or TIF2 L*XX*LL (Protein Data Bank access code 2Q7J) peptide superimpose to the DHT-bound structures with F*XX*LF (Protein Data Bank access code 1TR7) or L*XX*LL (Protein Data Bank access code 1T63) peptide (see Fig. 9) with an r.m.s.d. of 0.27 and 0.3 Å and to WT AR LBD-S-1 (Protein Data Bank access code 2AXA) and AR-W741L LBD-

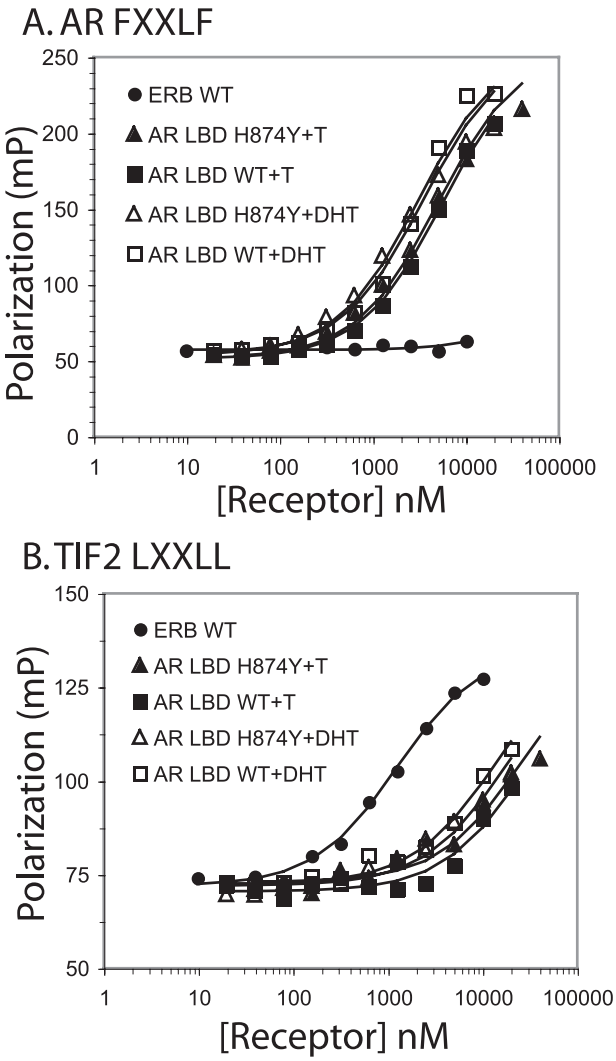

FIGURE 5. **Fluorescence binding isotherms.** *A,* increasing concentrations of AR LBD and AR-H874Y LBD purified in the presence of 10 μM T or DHT, and ERβ LBD in the presence of 40 μM estradiol were incubated for 1 h at room temperature without further ligand addition with fluorescein-labeled AR F*XX*LF peptide as described under "Experimental Procedures." *B,* increasing concentrations of purified WT AR LBD, AR-H874Y LBD, and ERβ LBD purified in the presence of 10 μM ligand were incubated for 1 h at room temperature in the presence of 40 μM T, DHT, or estradiol and fluorescein-labeled TIF2 L*XX*LL peptide as described under "Experimental Procedures." Affinity binding constants for AR F*XX*LF and TIF2 L*XX*LL peptides are summarized in Table 1. The data are the mean ± S.E. expressed as millipolarization units (*mP*) *versus* purified receptor LBD concentration.

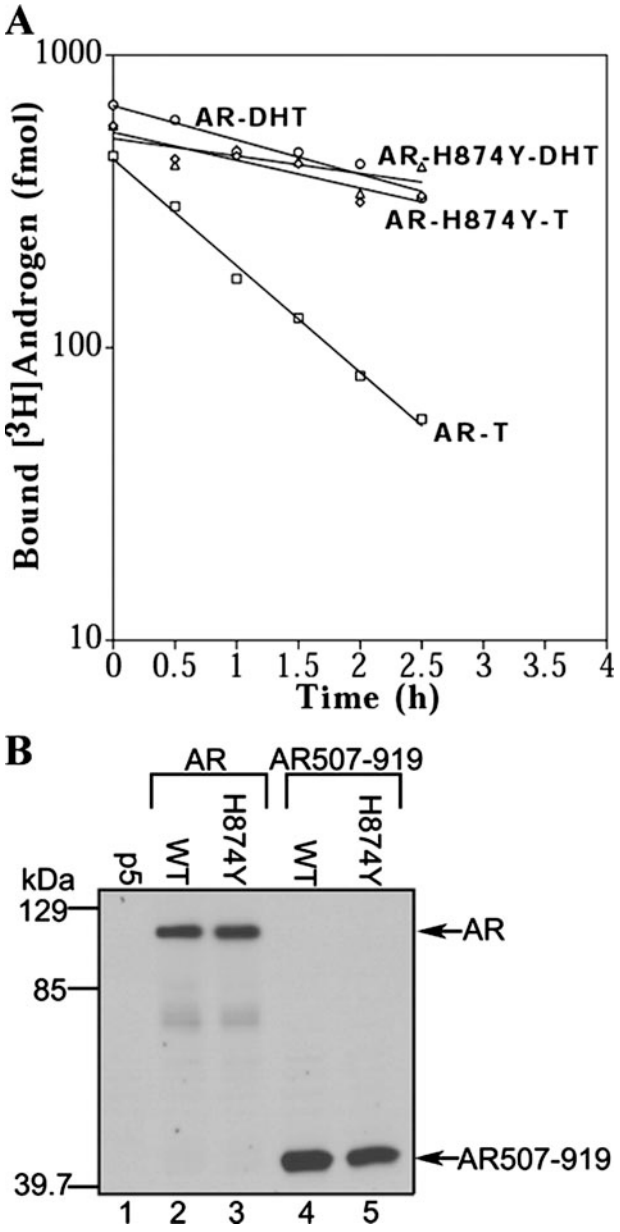

FIGURE 6. **Kinetics of T and DHT dissociation from AR and AR-H874Y.** *A,* dissociation rates of [^{3}H]T and [^{3}H]DHT were determined as described under "Experimental Procedures" by transient transfection of COS cells with 2 μg of pCMVhAR (AR) and 2 μg of pCMVhAR-H874Y (AR-H874Y). Transfected cells in culture were incubated for 2 h at 37 °C in the presence of 5 nM [^{3}H]T and 3 nM [^{3}H]DHT followed by a chase period with unlabeled 50 μM T or 50 μM R1881 and assayed at 30-min intervals up to 2.5 h. Pseudo-first order ligand dissociation allowed use of unlabeled R1881 to prevent rebinding of [^{3}H]DHT and avoid the complications of low water solubility of DHT. Dissociation half-times were calculated as the time required at 37 °C to reduce specific binding by 50%. Data are representative of three independent experiments. *B,* immunoblot of WT and H874Y AR and AR-(507–919) expression levels in COS cells. Cells transfected with 10 μg of pCMVhAR, pCMVhAR-(507–919), and the corresponding H874Y mutants were incubated in serum-free medium in the absence of hormone. Protein extracts (20 μg protein/lane) were separated on a 10% acrylamide gel containing SDS and the transferred protein blot probed using anti-AR antibody AR-52.

TABLE 1

Androgen-dependent AR LBD and AR-H874Y LBD binding affinities for AR F*XX*LF and TIF2 L*XX*LL peptides

Fluorescence polarization measurements were determined using fluorescein-labeled peptides as described under "Experimental Procedures" for 1 h at room temperature for purified AR LBD, AR-H874Y LBD, and ERβ LBD containing 10 μM T, 10 μM DHT, or 40 μM estradiol as indicated.

	T	DHT	E_2
F*XX*LF			
AR-LBD	5.5 ± 0.3	3.0 ± 0.4	
AR-LBD-H874Y	4.9 ± 0.6	3.5 ± 0.6	
ERβ-LBD			>30
L*XX*LL			
AR-LBD	27 ± 4	13.1 ± 1.5	
AR-LBD-H874Y	25 ± 5	17.2 ± 2.1	
ERβ-LBD			1.2 ± 0.1

bicalutamide (Protein Data Bank access code 1Z95) with an r.m.s.d. of 0.37 and 0.31 Å, respectively. Consistent with the AR LBD-R1881 (4) and DHT peptide bound structures (18, 42), the L*XX*LL motif in the T-bound structures is carboxyl-terminally shifted along the helical axis relative to the F*XX*LF peptide, and

TABLE 2

Dissociation half-times of [^{3}H]T and [^{3}H]DHT (min at 37 °C)

Dissociation rates of [^{3}H]T and [^{3}H]DHT from AR, AR-(507–919), and the corresponding H874Y mutants expressed from pCMV5 were determined in transfected COS cells at 37 °C as described under "Experimental Procedures." Dissociation half-times were calculated as the mean ± S.E. from at least three independent assays.

	T	DHT
AR	55 ± 6	188 ± 36
AR-H874Y	197 ± 27	268 ± 51
AR-(507–919)	25 ± 3	32 ± 4
AR-(507–919)-H874Y	49 ± 4	87 ± 6

Leu-745 and Leu-749 lie in register with Phe-23 and Phe-27 (Fig. 7*A*). The AR-(20–30) F*XX*LF peptide H-bonds to conserved charge clamp residues Glu-897 and Lys-720 required for AR AF2 activity (6). The NH_2 terminus of the L*XX*LL peptide fails to H-bond with Glu-897 and maintains the carboxyl-terminal shift, motif registry, and interaction to Lys-720 as shown for the AR LBD bound to R1881 (4) (Fig. 7, *A–C*). The T-bound ligand binding pockets are essentially identical to each other and nearly identical to the DHT-bound AR LBD structures (34, 42) (Fig. 7, *C* and *D*, and Table 4).

WT AR LBD-T-FXXLF and LXXLL—There were no major structural differences to thoroughly account for the noted physiologic differences between T and DHT. For both, the steroid A-ring lies near the side chain of Arg-752, a conserved helix-5 residue required for ligand binding (Fig. 8) (41, 43, 44). In the T-bound WT AR LBD-F*XX*LF structure, we observed a 3.0 Å interatomic distance between the steroid 3-keto O and Arg-752 side chain atom N-η2 and measured a 126° angle subtended by atoms Arg-752 N-η2, H-η22, and the T 3-keto O (Fig. 8*A* and Table 4). Although the 3.0 Å distance supports the presence of a direct H-bond with Arg-752, the angular displacement is less than the optimal 180° angle and only slightly more favorable than the 110°, 3.0 Å H-bond of DHT-AR LBD (Protein Data Bank access code 1T63) (Fig. 8, *B* and *C*).

Also located near the steroid A-ring is conserved structural water HOH1, which ideally could mediate up to four local H-bonds. However, three possible H-bond donors are side chain protons bonded to Arg-752 (N-η1 and N-η2) and Gln-711-A (N-ϵ2). Three possible H-bond acceptors[3] are Gln-711 (A) (O-ϵ1), the backbone carbonyl oxygen of Met-745 and the 3-keto O (Fig. 8*A*). Of these six atoms, the Arg-752 N-η2, Gln-711 N-ϵ2, and Met-745 backbone carbonyl oxygen align closest to three of four angles dictated by the tetrahedral geometry of water and leave open the possibility for HOH1 to donate an H-bond to the T 3-keto O. The likelihood of an HOH1 to 3-keto O H-bond is indicated by the reduced interatomic distance of 3.2 Å compared with 3.5 Å in DHT-bound structures (Protein Data Bank codes 1T63 and 1I37), the planar Δ4,5 double bond of T which positions the 3-keto O closer to HOH1, and the more negative charge character to the 3-keto O than the nonpolar neutral 3-keto O of DHT. The HOH1 to 3-keto O C3 vector of 117° is nearly colinear to 120° sp^2 electrons on the 3-keto O in favor of the HOH1 O-H vector. Although invoking an HOH1 to T 3-keto O H-bond forms a narrow 80° angle between the 3-keto O, HOH1 O, and Met-745 carbonyl oxygen atoms that violates the ideal tetrahedral water geometry, the superior hydrophilic properties of the T A-ring relative to DHT increase the propensity of T to accept this second H-bond through the fourth coordination of HOH1. Better H-bonding by T appears to also slightly reduce the distance between HOH1 and the Met-745 backbone carbonyl (2.7 Å) relative to DHT (2.9 Å).

On the D-ring of T, the 17β-hydroxyl group accepts an H-bond from the helix-10 Thr-877 side chain and donates an H-bond to helix-3 Asn-705 O-δ1 (Fig. 7*C* and Fig. 9) as reported for DHT and R1881 (4, 34). The Asn-705 side chain amine in turn H-bonds to the backbone carbonyl of Glu-890 in the linker between helix-11 and 12 (not shown). In the vicinity of the A-B-ring juncture, the C-19 bridgehead methyl group of T divides the hydrophobic space between Met-745 and Trp-741 as in the AR LBD-DHT structures and maintains the Trp-741 indole ring nitrogen rotated toward the conserved structural water (HOH3 in our WT AR structures) and residue 874.

Summarized here are amino acid residues in our T-bound structures where positive $3\sigma F_o - F_c$ electron density warranted the addition of a second side chain conformation or a sulfate ion. Occupancy for the A and B side chain conformers was to ~50% each, except for Gln-711, which was estimated as 80% A and 20% B at best: WT-T-F*XX*LF-Leu-712, Ser-740, Cys-806, Met-807, Ser-814, Ile-815, Met-895, and two sulfates; WT-T-L*XX*LL-Glu-678, Gln-711, Leu-712, Asn-727, Met-780, Cys-806, Ile-841, Met-895, and one sulfate; H874Y-T-F*XX*LF-Gln-711, Leu-712, Met-780, Cys-806, Ile-841, Met-895, and two sulfates; H874Y-T-L*XX*LL-Glu-678, Glu-709, Leu-712, Arg-726, Cys-806, and Met-895. Most notable among these is helix-3 Gln-711 near HOH1, the next sequential residue to Leu-712, which contacts $i + 1$ of the bound peptide motif, and helix-12 Met-895, which lies proximal to Leu-712 but more distal to the $i + 1$ residue of the bound peptide and the steroid A-ring (Fig. 10). We also observed in each structure, but do not illustrate, a glycerol that derives from the protein buffer solution that binds above the Gln-711 side chain. It is unclear whether these alternate conformers are crystallization artifacts or, as for Gln-711, arise from the presence of glycerol. Others such as Leu-712 or Met-895 may represent conformational freedom arising from a protein- or ligand-mediated mechanism.

AR H874Y LBD-T-FXXLF and LXXLL—We noted a more definitive structural change in our analysis of the AR-H874Y mutant LBD bound to T and AR F*XX*LF (Protein Data Bank access code 2Q7K) or TIF2 L*XX*LL (Protein Data Bank 2Q7L) peptide. Side chains of exterior helix-10 WT residue His-874 (Fig. 10*A*) and H874Y mutant residue Tyr-874 (Fig. 10*B*) occupy space in a second shell of residues that surround Met-742, a first shell interior helix-5 residue that contributes to the hydrophobic core and whose side chain lies adjacent to the steroid C-ring in the binding pocket. Side chains for Met-742 and third shell AF2 helix residues Val-903, Ile-906, and Leu-907 located above residue 874 are virtually superimposed atom for atom in the WT and H874Y structures (Fig. 10*D*), and the Met-

[3] Gln-711 side chain atoms O-ϵ1 and N-ϵ2 for both the A and B conformers were built as reported in the original WT AR LBD-DHT structure (34). Swapping these atom positions presents another possible H-bonding scheme such as that in the progesterone receptor (1A28 segid B) and AR (1E3G) and is not presented here.

TABLE 3
Crystallographic data and refinement statistics

Crystal	AR H874Y T AR-(20–30)	AR H874Y T TIF2-III	AR WT T AR-(20–30)	AR WT T TIF2-III
X-ray source/λ (Å)	APS-22BM/0.98	APS-17BM/0.98	APS-17BM/0.98	APS-17BM/0.98
Resolution (Å)	50.0-1.80	25.0-1.92	24.0-1.87	27.0-1.90
Space group	$P2_12_12_1$	$P2_12_12_1$	$P2_12_12_1$	$P2_12_12_1$
Unit cell (Å)	$a = 55.9$ $b = 66.1$ $c = 70.7$	$a = 54.4$ $b = 66.8$ $c = 69.9$	$a = 56.0$ $b = 66.4$ $c = 70.8$	$a = 54.8$ $b = 66.9$ $c = 70.2$
Unique reflections	24,591	20,085	22,190	20,937
Complete (%) (last shell)	98.5 (87.4)	99.5 (98.1)	98.6 (87.8)	99.9 (100.0)
I/σ (last shell)	41.1 (3.8)	41.6 (3.0)	41.9 (2.4)	47.4 (3.8)
R_{sym} [a] (%) (last shell)	4.2 (29.9)	4.7 (54.6)	4.4 (60.0)	4.4 (52.6)
Refinement	Refmac	Refmac	Refmac	Refmac
Resolution range	42.7–1.8	20.5–1.92	20.5–1.87	20.6–1.90
R_{factor} [b]/R_{free} [b] (%)	18.0/20.9	18.2/22.1	17.3/21.7	18.0/22.0
Bond lengths[c] (Å)	0.008	0.009	0.008	0.009
Bond angles[c] (°)	1.07	1.15	1.17	1.13
Mean *B* value	23.7	30.4	28.0	28.7
Non-hydrogen atoms	2265	2303	2275	2330
Protein/peptide	2058	2125	2055	2140
Ligand	21	21	21	21
Solvent/other	170/16	151/6	183/16	158/11
Protein Data Bank access code[d]	2Q7K	2Q7L	2Q7I	2Q7J

[a] $R_{sym} = \Sigma|I_{avg} - I_i|/\Sigma I_i$ is the data consistency, where I_{avg} is the mean observed intensity and I_i is the observed intensity.
[b] $R_{factor} = \Sigma||F_{obs} - F_{calc}|/\Sigma F_{obs}$, where F_{obs} and F_{calc} are the observed and calculated structure factors; R_{free} is calculated from 3.2% of randomly selected reflections excluded in refinement and R_{factor} calculations.
[c] Reported as the r.m.s.d. from ideal geometry.
[d] Structure coordinates and structure factor files are available at the Protein Data Bank web site.

742 side chain clearly conforms to a single orientation for WT and H874Y AR. This overall WT AR configuration allows structural HOH3 to mediate an H-bond network from the His-874 side chain (N-ϵ2) to the Met-742 backbone carbonyl and continues through HOH4 to the helix-4 Tyr-739 backbone carbonyl (Fig. 10*A*).

Despite the bulkier phenyl hydroxyl group, Tyr-874 in the H874Y mutant appears easily accommodated with no major rearrangement of neighboring helices or side chains (Fig. 10, *B* and *C*). Tyr-874 supplies a larger side chain that extends more than 2 Å further toward helix-5 and displaces HOH3 with its phenolic hydroxyl group and presents a definitive change in H-bonding scheme. The helix-10 Tyr-874 phenolic oxygen can accept a direct 3.4 Å H-bond from the backbone amide of helix-5 Met-742 at a favorable angle of 120° (Tyr-874 C-ζ, O-η to Met-742 N) that closely aligns the Met-745 amide N-H bond vector to the assumed 120° sp^2 electrons of the Tyr-874 O-η atom. In turn the Tyr-874 hydroxyl proton donates a 2.8 Å direct H-bond to the backbone carbonyl of helix-4 Tyr-739 at a favorable angle of 121° (Tyr-874 O-η to Tyr-739 O, C) that closely aligns with the assumed 120° sp^2 electrons of the Tyr-739 carbonyl O atom. It is noteworthy that helix-4 residue Tyr-739 is adjacent to Gln-738, a residue whose side chain lies adjacent to the $i + 1$ residue and displays different conformations with induced fit binding to the F*XX*LF or L*XX*LL motif and can participate in an H-bond network that links the helix-4 Met-734 CO to Lys-905 through the Gln-738 and Gln-902 side chains (Fig. 10*D*). The Tyr-874 phenyl presents more favorable side chain chemistry to engage C-δ2 and C-ϵ1 in hydrophobic interactions with Val-903 C-γ2 (3.5 Å) and Ile-906 C-δ1 (3.4 Å) than the heterocyclic imidazole ring of WT His-874 (4.0 Å from C-δ2 to Val-903 C-γ2 and 3.7 Å from C-ϵ1 to Ile-906 C-δ1) (Fig. 10*D*). The nearly identical T-bound crystal structures reveal that restored activation by T-bound AR-H874Y is not directly ligand-mediated or accompanied by T-induced structural rearrangement and must be driven by the H874Y mutation.

DISCUSSION

AR Activation by T and DHT—AR is unique among the family of steroid hormone receptors by having two biologically active high affinity hormones that differ in physiological potency. DHT is a morphogen required for male sexual developmental, whereas T is the major androgen in muscle and is anabolic at puberty. Normal levels of T without conversion to DHT fail to stimulate complete male genital development of the human fetus. This is evident from the human 5α-reductase syndrome caused by a genetic defect in the enzyme that converts T to DHT (46). Activity differences between T and DHT cannot be explained by differences in transcription targets because there is no compelling evidence for differentially regulated gene sets, nor are they explained by the often reported different AR binding affinities for T and DHT. True equilibrium binding conditions may not be uniformly established, because the ligand-free AR and AR bound to T are more susceptible to degradation than AR bound to DHT leading to overestimation of T binding affinity. By measuring association and dissociation rate constants and accounting for AR instability in the absence and presence of ligand, T and DHT equilibrium binding affinities are similar (1). Nevertheless, an ~10-fold higher concentration of T is required to achieve the AR mediated transcriptional effects of DHT (47). A DHT-like transcriptional response by higher concentrations of T is supported by the 5α-reductase gene knock-out mouse where a compensatory rise in circulating T levels results in masculinization at birth (48). Masculinization in humans with 5α-reductase deficiency occurs at puberty when circulating T levels increase (49).

In this study we sought to elucidate the molecular basis for the different activities of T and DHT. Our biochemical data show that relative to DHT, T is a less potent androgen because of weaker F*XX*LF and L*XX*LL motif interactions at AF2 that are increased by the H874Y mutation. T and DHT dissociate with

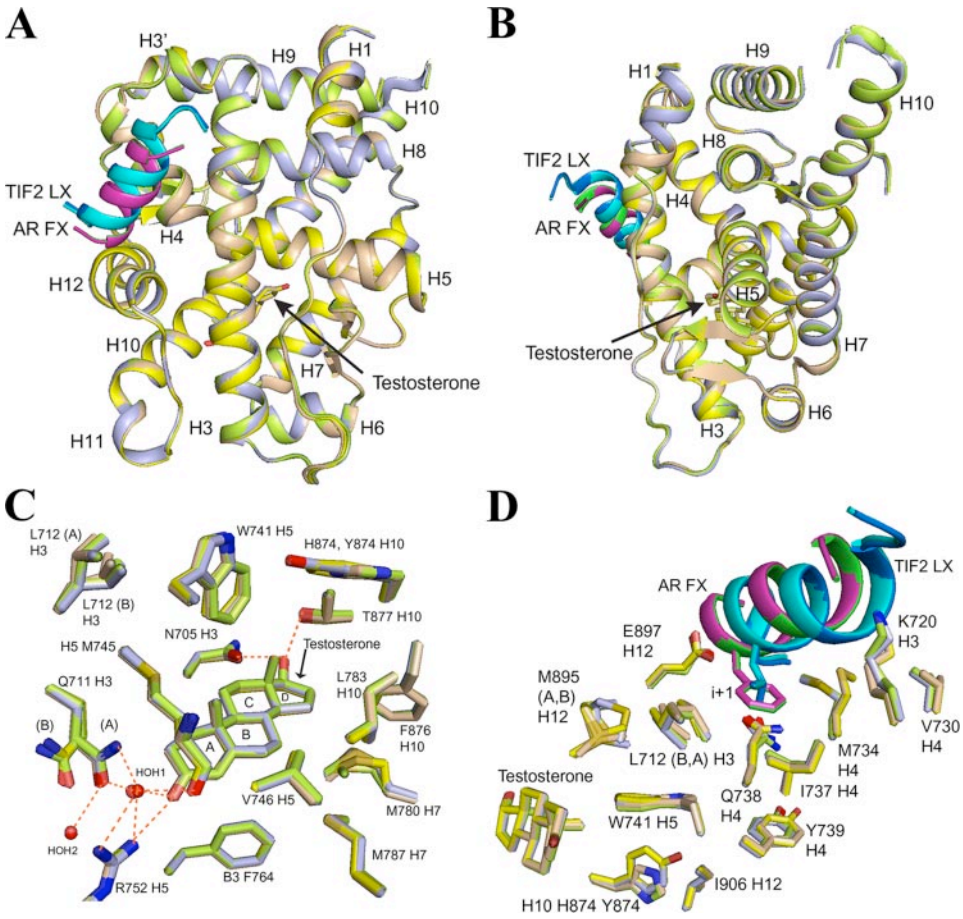

FIGURE 7. **Crystal structures of WT and H874Y AR LBD bound with T and AR F*XX*LF or TIF2 L*XX*LL peptide.** *A,* global front view of superimposed structures of WT and H874Y AR LBD bound to T and AR-(20–30) F*XX*LF or TIF2-(740–752) L*XX*LL peptide. Shown are WT AR LBD-T-AR F*XX*LF peptide (*tan,* LBD ribbon; *magenta,* peptide), WT AR LBD-T-TIF2 L*XX*LL peptide (*lime green,* LBD ribbon; *cyan,* peptide), H874Y AR LBD-T-AR F*XX*LF peptide (*yellow,* LBD ribbon; *green,* peptide) and H874Y AR LBD-T-TIF2 L*XX*LL peptide (*lavender,* LBD ribbon; *blue,* peptide), and T (LBD ribbon color carbon; *red,* oxygen). Human AR helix (*H*) and β-strand (*BS*) amino acid residues are H1 673–680; H2 not assigned; H3 697–721; H3′ 725–727; H4 730–739; H5 741–756; BS3 761–765; BS4 768–771; H6 772–776; H7 780–797; H8 801–812; BS5 815–817; H9 824–842; H10 851–882; H11 884–887; H12 893–908; BS6 911–913. *B,* rotated view of *A* looking toward the carboxyl-terminal end of helix-5 and NH_2-terminal ends of helices 6 and 8. Residues 843–850 between H9 and H10 were devoid of electron density. *C,* detailed view of the T-bound ligand binding pocket and surrounding residues of WT and H874Y AR LBD bound with AR-(20–30) F*XX*LF or TIF2-(740–752) L*XX*LL peptide. In all four T-bound structures the ligand binding pockets are essentially identical to each other. A single conformation was observed for all the displayed side chains except for Leu-712 (50%, *A* and *B*) and Gln-711 (80%, *A* and 20%, *B* in the WT AR LBD-T-L*XX*LL and AR-H874Y LBD-T-F*XX*LF structures). A buffer-derived glycerol molecule (not shown) near Gln-711 was present in all four WT and H874Y AR LBD-T structures. Color scheme as in *A* with nitrogen atoms in *blue* and oxygen atoms in *red*; *orange dashed lines* designate potential interactions with neighboring polar atoms. *D,* detailed view to display the molecular architecture from the ligand binding pocket to the AF2 peptide-binding site and *i* + 1 side chain of Phe-23 of bound AR-(20–30) F*XX*LF peptide and Leu-745 of bound TIF2 L*XX*LL peptide. Different conformers of Met-734 and Tyr-739 correlate with the induced fit binding of the F*XX*LF or L*XX*LL motif. The WT and H874Y AR LBD bound to T and AR F*XXLF* or TIF2 L*XXLL* peptide are superimposed and use the color scheme of *A*. Side chains for Leu-712 and Met-895 are distributed equally into two rotamers.

ligands transmit different signals to the AF2 surface. Our structural data suggest that differences in A-ring H-bonding alter the conformational freedom of neighboring AF2 floor residue Leu-712. Structures of T-bound AR-H874Y indicate a gain-of-function arising not from chemical differences between T and DHT or altered motif binding affinity, but from replacement of a water-mediated H-bond network with direct H-bonds between external helix-10 Tyr-874 side chain and internal helix-4 Tyr-739 and helix-5 Met-742 backbone atoms. For both WT AR and AR-H874Y, small changes in H-bonding have measurable effects on motif binding at AF2 and ultimately AR transcriptional activity.

Chemical Properties of T and DHT—T is the major circulating male hormone and like DHT has 19 carbons and differs only by a Δ4,5 double bond in ring A. With two fewer protons than the saturated ring A of DHT, the Δ4,5 double bond of T polarizes the region and increases the negative charge at the 3-keto O and positive charge at carbon 5. Based on Coulomb's law for simple electrostatic interactions (50), these properties of T impart greater H-bonding potential that accounts for its 10-fold greater water solubility than DHT. However, water solubility and inherent hydrophilicity and hydrophobicity do not explain androgen retention times in the binding pocket because T, DHT, and R1881 dissociate with similar rates from an AR fragment containing the LBD, and R1881 dissociates from AR at a rate intermediate between T and DHT (7). Water solubility and dissociation rate of R1881 similar rates from AR-(507–919), but T dissociates ~3 times faster than DHT from WT AR and considerably slower from AR-H87Y. These results indicate that weaker AR F*XX*LF motif binding to AF2 results in the more rapid dissociation of T. Conversely, stronger AR F*XX*LF motif binding slows DHT dissociation from WT AR and T and DHT dissociation from AR-H874Y. Weaker interactions at AF2 thus appear to explain the reduced androgenic activity of T.

The similar LBD crystal structures of T-bound WT AR LBD with AR F*XX*LF or TIF2 L*XX*LL peptide to that of DHT (18, 34, 42) provide only subtle clues how these chemically similar are further influenced by a 17-methyl group on ring D that introduces more hydrophobic character to a hydrophobic pocket near Met-780, Leu-704, and Leu-701.

In the same sense, the saturated nonpolar ring A of DHT is more chemically compatible with the hydrophobic environment of proximal ligand binding pocket residues than the unsaturated polar A-ring of T. Phe-764 is a conserved hydrophobic residue among steroid receptors (41) along with Val-746, Met-749, Leu-704, and Leu-707 that contact the bound ligand. Compared with T, the greater hydrophobic character and complementary shape of the DHT A-ring cannot explain

TABLE 4

Hydrogen bond distances and angles for WT AR LBD bound with T and AR F*XX*LF peptide or DHT and L*XX*LL peptide

Gln-711 N is oriented up for WT AR LBD-T with AR-(20–30) F*XX*LF peptide (Protein Data Bank code 2Q7I) and WT AR LBD-DHT with ARA70 F*XX*LF peptide (Protein Data Bank code 1T63) (42) consistent with the original AR LBD-DHT structure (34). Distances and angles were measured by PyMol from heavy atom (H), proton (P), carbonyl oxygen (CO), carbonyl oxygen, or carbon (C), heavy atom to heavy atom (H2H), heavy atom to proton (H2P). Ideal water geometry is tetrahedral with ~109° angles.

WT AR LBD-T-F*XX*LF

	BOND DISTANCE (A)				BOND ANGLE (°)				
	ATOM	ATOM	H2H	H2P	ATOM	ATOM	ATOM	H2H2H	H2P2H
H bonds	HOH1	M745O	2.7	–	HOH1	M745O	M745C	–	117
	R752Nη2	T-O3	3.0	2.3	R752Nη2	H	T-O3	126	–
	HOH1	T-O3	3.2	–	HOH1	T-O3	T-C3	–	117
	R752Nη1	HOH1	3.0	2.0	HOH1	H	R752Nη1	151	–
	Q711Nε2	HOH1	2.6	1.8	Q711Nε2	H	HOH1	142	–
	HOH2	Q711O	3.0	–	HOH2	Q711O	Q711C	–	146
Alternate	R752Nη2	HOH1	3.1	2.2	R752Nη2	H	HOH1	145	–
Potential	HOH1	Q711O	3.4	–	HOH1	Q711O	Q711C	–	77
Interactions	HOH2	F764O	2.7	–	HOH2	F764O	F764C	–	143
	Q711Nε2	T-O3	3.7	3.0	Q711Nε2	H	T-O3	127	–

				H2H	H2P (P2P*)
HOH1 Geometry	3-keto O	HOH1	R752Nη1	102	112
	R752Nη1	HOH1	Q711Nε2	117	128*
	Q711Nε2	HOH1	T-O3	78	67
	Q711Nε2	HOH1	M745O	124	112
	M745O	HOH1	R752Nη1	117	119
	M745O	HOH1	T-O3	80	–

WT AR LBD-DHT-L*XX*LL

	BOND DISTANCE (A)				BOND ANGLE (°)				
	ATOM	ATOM	H2H	H2P	ATOM	ATOM	ATOM	H2H2H	H2P2H
	HOH1	M745O	2.9	–	HOH1	M745O	M745O	–	117
	R752Nη2	T-O3	3.0	2.5	R752Nη2	H	T-O3	110	–
	R752Nη1	HOH1	3.1	2.2	R752Nη2	H	HOH1	151	–
	Q711Nε2	HOH1	2.7	1.9	Q711Nε2	H	HOH1	135	–
	HOH2	Q711O	3.1	–	HOH2	Q711O	Q711C	–	137
	R752Nη2	HOH1	3.0	2.1	R752Nη1	H	HOH1	145	–
	HOH1	Q711O	3.4	–	HOH1	Q711O	Q711C	–	79
	HOH1	T-O3	3.5	–	HOH1	T-O3	T-C3	–	100
	HOH2	F764O	2.9	–	HOH2	F764O	F764C	–	143
	Q711Nε2	T-O3	4.0	3.3	Q711Nε2	H	T-O3	128	–

				H2H	H2P (P2P*)
	M745O	HOH1	R752Nη1	116	116
	R752Nη1	HOH1	Q711Nε2	121	134*
	Q711Nε2	HOH1	M745O	122	108
	Q711Nε2	HOH1	T-O3	79	68
	M745O	HOH1	T-O3	79	–
	R752Nη1	HOH1	T-O3	98	109

the slower dissociation rate of DHT from full-length AR because T and DHT dissociate with similar rates from AR-(507–919). On the other hand, the saturated A-ring of DHT may more effectively increase AR AF2 activity by stabilizing the LBD core for higher affinity motif interactions.

Counterintuitive Hypothesis for T and DHT Activity—Modulation of F*XX*LF or L*XX*LL motif binding at AF2 by T and DHT relies on a conserved H-bond between Arg-752 N-η2 and the steroid 3-keto O which is influenced by the Δ4,5 double bond in T that imposes a more planar nature to the double bond side of ring A. Our T structures display a 3.0 Å H-bond heavy atom distance from the ring A 3-keto O to Arg-752 the same as DHT, but an angle from the more planar A-ring of T (126°) that is slightly more favorable for H-bonding than the chair configuration in DHT (110°) (Fig. 8, *A*–*C*). This contrasts a recent report indicating a better Arg-752 to 3-keto O H-bond for DHT than T (51).

Ring A chemistry also influences a network of H-bonds through structural water HOH1 that is centrally positioned between ring A of T and key residues in AF2 backbone helices 3 and 5. HOH1 can accept a proton from side chains of helix-5 Arg-752 (3.0 Å) and helix-3 Gln-711 (2.6 Å) and donate a proton to the backbone carbonyl of helix-5 Met-745 (2.7Å).[3] Based on the distance and angular relationships, these H-bond interactions for bound T and DHT satisfy 3 of 4 possible tetrahedral coordinates to water (52). T appears more likely than DHT to also accept an H-bond from HOH1 because of the more planar Δ4,5 double bond in ring A positions the 3-keto O of T 0.3 Å closer to HOH1 and the greater negative charge centered on the 3-keto O of the dipolar A-ring. The 117° angle for the assumed HOH1 O H-bond vector of T aligns well with the 120° sp^2 3-keto O electrons compared with 100° for DHT (53). The polar nature and superior hydrophilic properties of the T A-ring over DHT may favor the coexistence of donated H-bonds from HOH1 to the 3-keto O and Met-745 despite formation of a nonideal, constrained 80° angle (T 3-keto O, HOH1, Met-745 O) within the tetrahedral geometry of HOH1.

Our results suggest the counterintuitive hypothesis that greater H-bonding by T is detrimental to agonist activity. With shorter distances between HOH1 and the 3-keto O and Met-745 carbonyl and the negative charge character of its 3-keto O, the polarized A-ring of T may over-constrain the geometry and introduce unfavorable hydrophilic character into the hydrophobic environment of the binding pocket. The T Δ4,5 polarized double bond is located in a hydrophobic region bounded by Met-745, Phe-764, Met-749, and Val-746 within 5 Å of the Met-745 to Val-746 amide bond. This introduces a polar atom mismatch with the 3-keto O being 3.8 Å to the Met-745 O and the presumably positive T C-5 atom within 5 Å of the Val-746 NH. In contrast, through changes also not evident in the crystal structures, it was recently suggested that a novel high affinity nonsteroidal AR modulator may influence AF2 activity by engaging more favorable hydrophobic π-bonding to Phe-764 and alternative H-bonding to backbone residues in helices 3 and 5 (45).

For DHT, the nonpolar saturated boat-configured A-ring provides a neutral 3-keto O and increases the distance between HOH1 and the 3-keto O to 3.5 Å, which weakens or eliminates a second HOH1-mediated H-bond. More relaxed A-ring geometry of DHT is further evident in the 0.2 Å longer distance between HOH1 and the Met-745 O. The saturated A-ring of DHT eliminates the polarized atom mismatch and provides better hydrophobic interactions with neighboring residues listed above. Just exactly how T and DHT transmit these different signals to the AF2 surface is not clear, but in both cases the side chain of Met-745 lies above the steroid A-ring and projects toward Leu-712, a proximal residue that lies in the floor of AF2.

AF2 Residue Leu-712—Leu-712 establishes key hydrophobic contacts with $i + 1$ Phe-23 of the AR $F_{i+1}XXLF$ motif and $i + 1$ Leu-745 of the TIF2 L*XX*LL motif. Physiological relevance for Leu-712 in AR activity is established by the L712F mutation that causes grade 3 partial androgen insensitivity without altering equilibrium androgen binding affinity (7, 54). Increased bulk by Phe-712 in AR-L712F may interfere at the $i + 1$ motif-binding site. Low intensity difference map electron density

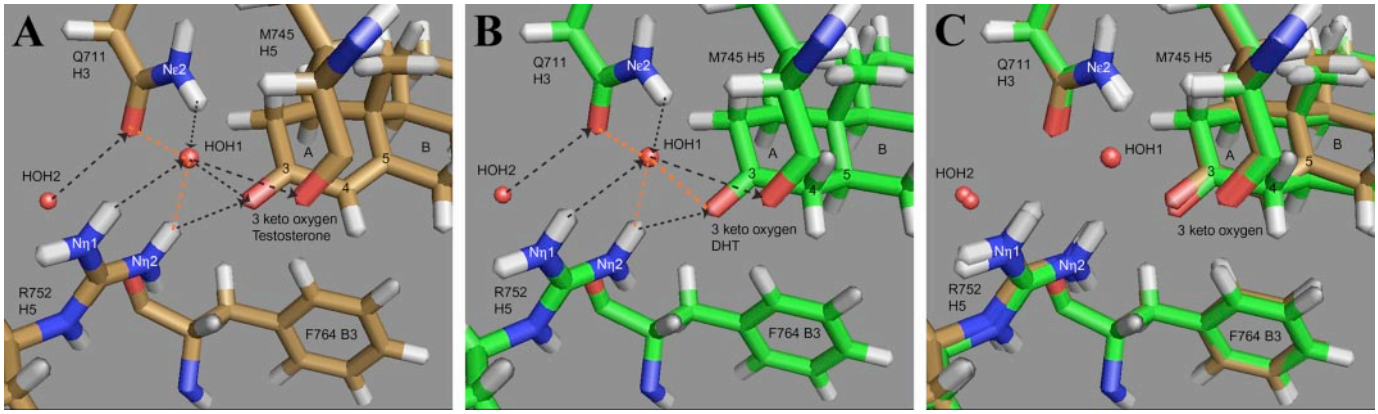

FIGURE 8. **Potential A-ring and water mediated H-bonding schemes for T and DHT.** Predicted A-ring H-bond distances and angles are shown based on the tetrahedral geometry of conserved structural water HOH1 (see Footnote 3 and see Table 4). *Arrowhead with black dashed lines* indicate the direction of donated H-bonds and *orange dashed lines* designate potential interactions with neighboring polar atoms of WT AR LBD bound to T and AR-(20–30) F*XX*LF peptide (*tan*) (*A*); WT AR LBD bound to DHT and GRIP-1-(740-752) L*XX*LL peptide (*green*) (42) (*B*); and the superimposition of *A* and *B* (*C*). Superior hydrophilic properties and a shorter distance are thought to enhance the HOH1 to T 3-keto O H-bond over that in DHT.

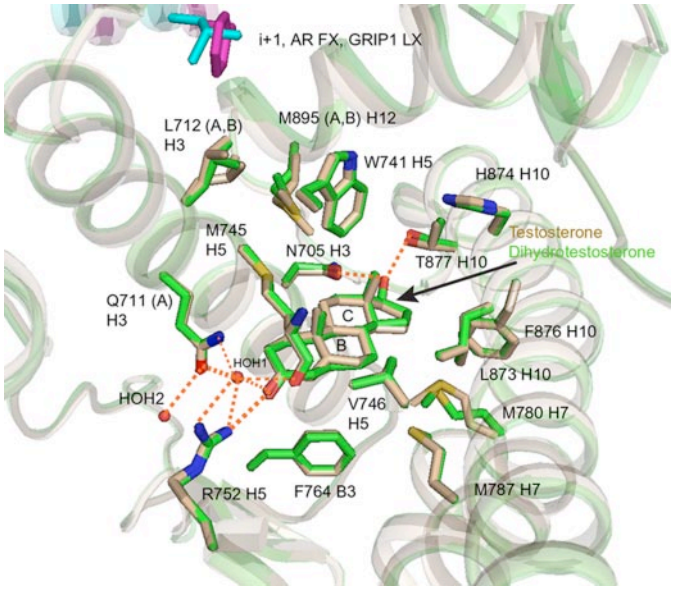

FIGURE 9. **Comparison of WT AR LBD-T-AR F*XX*LF and WT AR LBD-DHT-L*XX*LL.** Detailed view shows nearly identical molecular architecture of T and DHT-bound AR LBD from the ligand binding pocket to AF2 peptide-binding site. Shown here for WT AR LBD-T-AR-(20–30) F*XX*LF peptide (*tan*) but seen in all of our T-bound AR LBD structures are the two side chain conformations for Leu-712 and Met-895. By comparison with previously reported WT AR LBD-DHT (*green*) with GRIP-1-(740–752) L*XX*LL peptide (IT63, 42) or F*XX*LF (not shown, ITR7, 18), those side chains were conformed into a single rotamer. The $i + 1$ motif residues, Phe-23 (*magenta*) of the AR F*XX*LF peptide and Leu-745 (*cyan*) of the GRIP-1 L*XX*LL peptide, are shown. *Orange dashed lines* designate potential interactions with neighboring polar atoms. Portions of the LBD backbone are transparently displayed.

indicates the Leu-712 side chain is equally positioned in two conformations in all of our T-bound crystal structures. Two conformers are also seen with Met-895, an AF2 helix-12 residue within ~4 Å of Leu-712, but more distant to the $i + 1$ and steroid A-ring binding sites. Notably, there were single conformers of Leu-712 and Met-895 for WT AR LBD bound to DHT with F*XX*LF or L*XX*LL peptide (18, 34, 42).

We cannot rule out the possibility that the two conformations of Leu-712 and Met-895 are crystallographic artifacts. On the other hand, the better interactions between the 3-keto O of T to HOH1 and HOH1 to Met-745 and the polarity mismatch in the hydrophobic region near steroid carbons C-4 and C-5 suggest a mechanism not directly discerned from the structure. The effects of T appear to transmit through Met-745 to nearest AF2 floor residue Leu-712, which contacts the $i + 1$ residue of the bound peptide. Based on proximity to the A-ring and HOH1, the signaling conduit transmits through Gln-711 and/or Met-745 to Leu-712. Of these, Met-745 is most likely because it lies above the T A-ring Δ4,5 double bond to directly transmit A-ring chemistry to the side chain position of Leu-712 (Fig. 8). Gln-711 (adjacent to Leu-712) is less likely because two conformers of Gln-711 were in only two of four T-bound structures and was possibly influenced by a spuriously bound buffer-derived glycerol. More importantly, two conformers of Gln-711 were reported for WT AR bound to DHT and F*XX*LF peptide (18). Two conformations of Met-895 may be a more indirect contributor to AF2 or have a cross-helix influence from Leu-712. In contrast, DHT appears to impart greater structural integrity to Leu-712 and AF2 helix-12 Met-895 in and near AF2 allowing near maximum motif binding and AR transcriptional activity. Elimination of conformational heterogeneity in Leu-712 and Met-895 by DHT may be required for optimal AF2 activity.

There are examples where side chain conformations of ligand binding pocket residues are strongly influenced by chemical architecture of the bound ligand. The C-19 methyl group of T (shown here) and DHT (34) direct the side chains of Met-745 and Trp-741 into identical positions relative to the binding pocket. The Trp-741 nitrogen in the T and DHT-bound structures may establish interactions with structural HOH3. In contrast, R1881 lacks a C-19 methyl group, which allows Trp-741 the conformational freedom[4] to adopt a position where the indole nitrogen is rotated away from HOH3 (4, 7) as shown in Fig. 11. Nonsteroid ligands such as bicalutamide (44) or its S-1 agonist analog (43) extend ether linked para-substituted phenyl groups into an open channel between the

[4] Further evidence in the conformational freedom of Trp-741 is seen in our unpublished results with R1881, where this side chain is equally distributed between one rotamer close in orientation to that in the T and DHT structures and the other as shown in Fig. 11 (R. T. Gampe, Jr., unpublished results).

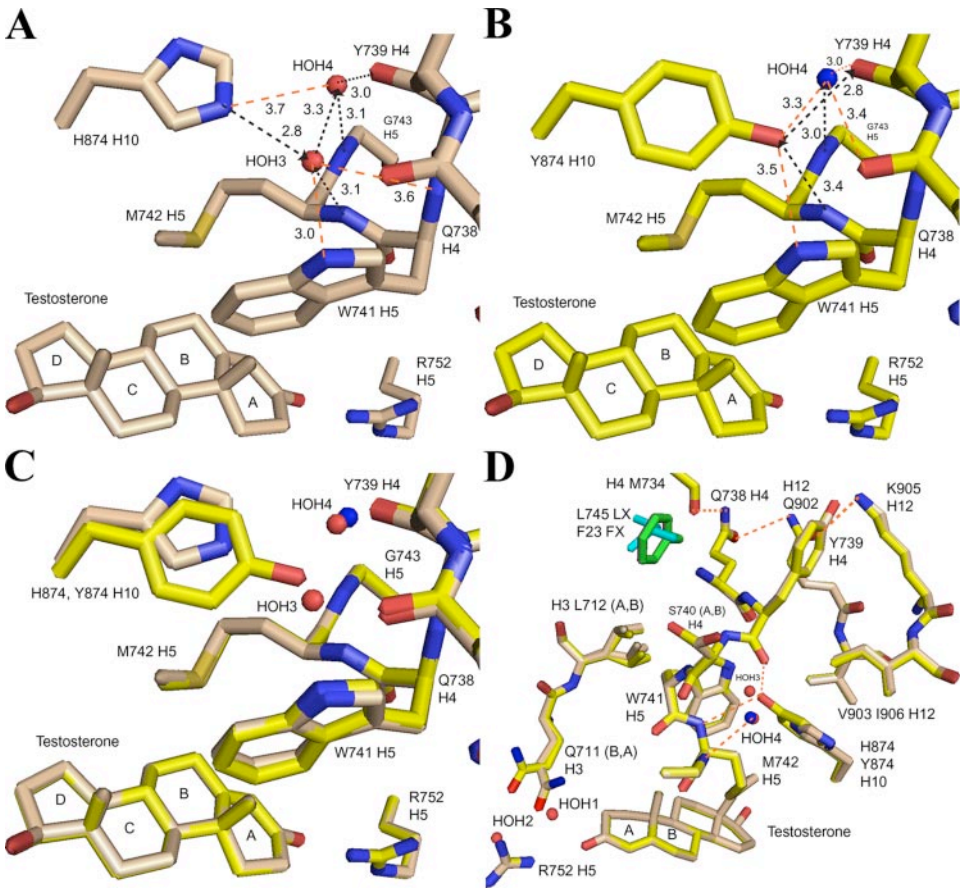

FIGURE 10. **Detailed crystal structure comparison of WT and H874Y AR LBD bound to T and AR F*XX*LF peptide.** *A,* detailed view of WT AR LBD bound to T and AR-(20–30) F*XX*LF peptide showing a water-mediated H-bond network from His-874 (*tan*) nitrogen (*blue*) through HOH3 (*red sphere*) to the helix-5 Met-742 amide and HOH4 to the helix-4 Tyr-739 backbone carbonyl. These conserved receptor core structural waters link His-874, which lies beneath helix-12, to Tyr-739. *Arrowhead with black dashed lines* indicate the direction of donated H-bonds; *orange dashed lines* designate potential interactions with neighboring polar atoms; interatomic distances are reported in Angstroms; T rings are labeled *A–D*. *B,* detailed view of AR-H874Y LBD-T-AR-(20–30) F*XX*LF peptide. Note the extended phenolic hydroxyl of AR H874Y prostate cancer mutation Tyr-874 displaces structural water HOH3 and provides direct H-bonds to the backbone amide of helix-5 Met-742 and the carbonyl of helix-4 Tyr-739 (*yellow*). H-bonds labeled as in *A* with HOH4 shown as *blue sphere*. *C,* superposition of *A* and *B* showing how the phenolic hydroxyl group of helix-10 mutant Tyr-874 of AR-H874Y nearly extends to the same position as HOH3 in the WT AR LBD structure with conservation of backbone positions for Tyr-739, Trp-741, and Arg-752. *D,* superposition of WT AR LBD (*tan*) bound to T and AR-(20–30) F*XX*LF ($i + 1$ Phe-23, *green*) and AR-H874Y LBD (*yellow*) bound to T and AR-(20–30) F*XX*LF ($i + 1$ Phe-23, *magenta*). TIF2-(740–752) L*XX*LL $i + 1$ residue Leu-745 (*cyan*) is shown for comparison. Direct H-bonding by Tyr-874 to the backbone of Tyr-739 displaces HOH3 and could further stabilize another H-bonding network represented with *orange dashed lines* that links Met-734 CO to Gln-738, Gln-902, and Lys-905.

AF2 helix-12 Met-895 and helix-5 Met-742 and cause Trp-741 to adopt yet a third unique conformation (Fig. 11).

Prostate Cancer Mutant AR-H874Y—H874Y is an AR somatic mutation identified in the human CWR22 prostate cancer xenograft that was isolated from a hormone refractory bone marrow metastasis of a patient treated with flutamide and luteinizing hormone-releasing factor agonist (24) and in a bone marrow metastasis from another patient receiving similar treatment (55). AR-H874Y retains high affinity T and DHT binding (7, 56) but more effectively interacts with the F*XX*LF motif despite similar motif binding affinity to WT AR. Improved F*XX*LF motif binding contributes to the slower dissociation rate of T and nearly equivalent T-induced transcriptional response as DHT-bound WT AR. Optimal AR F*XX*LF motif binding and slow ligand dissociation are thus hallmarks of the fully stabilized AR consistent with properties of the AR N/C interaction (8, 57) and AR stabilization (7, 58). Greater AF2 activity of T-bound AR-H874Y is supported by the effects of MAGE-11, an AR coregulator that binds the AR F*XX*LF motif and targets AF2 for activation by SRC/p160 coactivators (23).

The nearly identical crystal structures of bound T and DHT and surrounding pocket residues indicate that the DHT-like activity of T-bound AR-H874Y is not strictly ligand-mediated. H874Y provides two direct H-bonds in the receptor core in place of three water-mediated H-bonds in WT AR LBD that can stabilize the interior core near helix-5 Met-742, helix-4 Tyr-739, and exterior helix-10 that underlies AF2 helix-12. This tethers Met-742, a key residue proximal to the ligand binding pocket, and Tyr-739 near key AF2 domain residues, with exterior helix-10 via the mutant Tyr-874. Direct H-bonding likely improves AF2 motif binding and increases the lifetime of bound T. Agonist-induced stabilization of helix-10 is supported by the activity of S-1 bicalutamide that may form an H-bond from its fluorine atom to HOH3, a structural water that interacts with His-874 and is functionally replaced by the Tyr-874 phenolic oxygen (see Fig. 11) (43). The proposed destabilizing effects of T are more than compensated by the structural stabilizing effects of the H874Y mutation. Increased activity by AR-H874Y was also recognized for hydroxyflutamide and other ligands (24, 43). AR mutations that cause the androgen insensitivity syndrome support the importance of stabilizing helix-10 for AR function as well (59).

Prostate cancer cell survival and tumor expansion is favored by mutations that increase AR response to T, particularly in recurrent prostate cancer where SRC/p160 coactivators can be overexpressed (22). Our studies provide support for recent findings that local androgen production increases AR transcriptional activity in prostate cancer. Greater circulating T levels correlate with prostate cancer development (60, 61) and unlike normal prostate following androgen deprivation (62), T levels persist in recurrent prostate cancer tissue (63).

H-bond Chemistry and Protein Structure—Subtle changes in water-mediated H-bond chemistry that influence AR transcriptional activity may result from thermodynamic effects on protein structure and protein-ligand interactions (64).

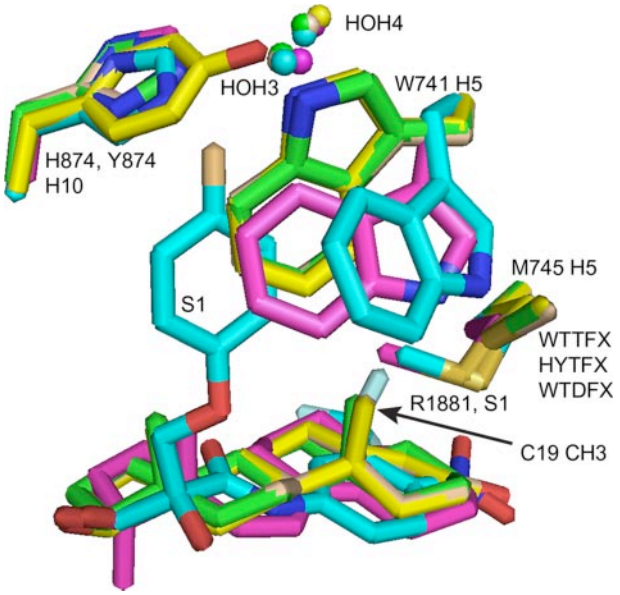

FIGURE 11. **Structural differences between the steroid and nonsteroidal ligand binding pockets.** Superimposition of WT AR LBD crystal structures bound with an F*XX*LF peptide and T (*brown*), DHT (*green*) (18), R1881 (*magenta*) (4), and S-1 bicalutamide agonist analog (*cyan*) (43) and AR-H874Y LBD bound to the AR F*XX*LF peptide and T (*yellow*). The C-19 bridgehead methyl group on T and DHT forces the Met-745 and Trp-741 side chains away from the steroid A-ring. For R1881 and S-1, the absence of an equivalent methyl group allows these side chains to adopt different rotamers that fill the vacated space above ring A[4]. The *para*-fluoro phenyl group on S1 extends into the space between helix-12 Met-895 and helix-5 Met-742 and directs Trp-741 to a third unique conformation. Appropriate *para*-phenyl substituents are thought to stabilize the AR LBD core by interacting with HOH3 (43).

H-bonds between protein groups and buried water molecules can stabilize structure through compensatory changes in enthalpy and entropy (65) as might occur for the H-bonding projections of Gln-711, Arg-752, Met-745, His-874, and Tyr-874. Such water-mediated H-bonds can provide favorable enthalpy but less favorable entropy than direct H-bonds in protein-ligand interactions (64, 66). Deeply buried structured water molecules engaged in multiple H-bonds increase protein flexibility and vibrational entropy, whereas direct protein-mediated H-bonds provide a more rigid structure with fewer degrees of freedom compared with water-mediated H-bonds (67). Replacement of structured water by direct H-bonds in AR-H874Y may reduce vibrational entropy and stabilize AF2 helix-12 for improved F*XX*LF and L*XX*LL motif binding (5, 7). Increased stabilization of AF2 helix-12 by direct H-bonding in AR-H874Y could increase the activity of T and weaker adrenal androgens. Nonsteroidal ligands such as bicalutamide or the S-1 analog have an extended *para*-phenyl substituent that binds in a channel between AF2 and His-874 that can directly H-bond to the same HOH3 through a fluorine atom (43, 44).

We conclude that T and DHT differentially modulate AR activity by altering the AR AF2 surface response toward AR F*XX*LF and coactivator L*XX*LL motif binding mediated through a network of water-mediated H-bonds and hydrophobic interactions. T-bound WT AR acquires subtle conformational instability arising from the increased polarity of T, which decreases the effectiveness of AF2 to serve as an F*XX*LF and L*XX*LL motif-binding site. DHT-bound WT AR and prostate cancer mutant AR-H874Y bound to T or DHT fully engage the F*XX*LF and L*XX*LL motifs for maximal AR transcriptional activity. The biologically active androgens T and DHT are examples of agonist-dependent modulation of AF2 transcriptional activity that has profound physiological consequences *in vivo*.

Acknowledgments—We thank John T. Minges, Andrew T. Hnat, Brian J. Kennerley, and K. Michelle Cobb for excellent technical assistance. We also thank Jan Hermans, Frank S. French, Shawn P. Williams, Lee F. Kuyper, Eugene L. Stewart, and Robert T. Nolte for helpful discussions, and we acknowledge Shawn P. Williams and Kevin P. Madauss for data collection at SER-CAT. Use of the IMCA-CAT beamline 17-BM at the Advanced Photon Source was supported by the companies of the Industrial Macromolecular Crystallography Association through a contract with the Center of Advanced Radiation Sources at the University of Chicago. Use of the Advanced Photon Source was supported by the United States Department of Energy, Office of Science, Office of Basic Energy Science, under Contract W-31-109-Eng-38.

REFERENCES

1. Wilson, E. M., and French, F. S. (1976) *J. Biol. Chem.* **251,** 5620–5629
2. Simental, J. A., Sar, M., Lane, M. V., French, F. S., and Wilson, E. M. (1991) *J. Biol. Chem.* **266,** 510–518
3. Warnmark, A., Treuter, E., Wright, A. P., and Gustafsson, J. A. (2003) *Mol. Endocrinol.* **17,** 1901–1909
4. He, B., Gampe, R. T., Kole, A. J., Hnat, A. T., Stanley, T. B., An, G., Stewart, E. L., Kalman, R. I., Minges, J. T., and Wilson, E. M. (2004) *Mol. Cell* **16,** 425–438
5. He, B., Kemppainen, J. A., and Wilson, E. M. (2000) *J. Biol. Chem.* **275,** 22986–22994
6. He, B., and Wilson, E. M. (2003) *Mol. Cell. Biol.* **23,** 2135–2150
7. He, B., Gampe, R. T., Hnat, A. T., Faggart, J. L., Minges, J. T., French, F. S., and Wilson, E. M. (2006) *J. Biol. Chem.* **281,** 6648–6663
8. Langley, E., Zhou, Z. X., and Wilson, E. M. (1995) *J. Biol. Chem.* **270,** 29983–29990
9. Schaufele, F., Carbonell, X., Guerbadot, M., Borngraeber, S., Chapman, M. S., Ma, A. A., Miner, J. N., and Diamond, M. I. (2005) *Proc. Natl. Acad. Sci. U. S. A.* **102,** 9802–9807
10. He, B., Lee, L. W., Minges, J. T., and Wilson, E. M. (2002) *J. Biol. Chem.* **277,** 25631–25639
11. Li, J., Fu, J., Toumazou, C., Yoon, H. G., and Wong, J. (2006) *Mol. Endocrinol.* **20,** 776–785
12. Hsu, C. L., Chen, Y. L., Ting, H. J., Lin, W. J., Yang, Z., Zhang, Y., Wang, L., Wu, C. T., Chang, H. C., Yeh, S., Pimplikar, S. W., and Chang, C. (2005) *Mol. Endocrinol.* **19,** 350–361
13. Langley, E., Kemppainen, J. A., and Wilson, E. M. (1998) *J. Biol. Chem.* **273,** 92–101
14. He, B., Kemppainen, J. A., Voegel, J. J., Gronemeyer, H., and Wilson, E. M. (1999) *J. Biol. Chem.* **274,** 37219–37225
15. Quigley, C. A., Tan, J. A., He, B., Zhou, Z. X., Mebarki, F., Morel, Y., Forest, M., Chatelain, P., Ritzen, E. M., French, F. S., and Wilson, E. M. (2004) *Mech. Ageing Dev.* **125,** 683–695
16. Ghali, S. A., Gottlieb, B., Lumbroso, R., Beitel, L. K., Elhaji, Y., Wu, J., Pinsky, L., and Trifiro, M. A. (2003) *J. Clin. Endocrinol. Metab.* **88,** 2185–2193
17. Quigley, C. A., De Bellis, A., Marschke, K. B., El-Awady, M. K., Wilson, E. M., and French, F. S. (1995) *Endocr. Rev.* **16,** 271–321
18. Hur, E., Pfaff, S. J., Payne, E. S., Gron, H., Buehrer, B. M., and Fletterick, R. J. (2004) *Plos Biol.* **2,** E274
19. He, B., Minges, J. T., Lee, L. W., and Wilson, E. M. (2002) *J. Biol. Chem.* **277,** 10226–10235
20. Hsu, C. L., Chen, Y. L., Yeh, S., Ting, H. J., Hu, Y. C., Lin, H., Wang, X., and Chang, C. (2003) *J. Biol. Chem.* **278,** 23691–23698

21. Chang, C. Y., Abdo, J., Hartney, T., and McDonnell, D. P. (2005) *Mol. Endocrinol.* **19,** 2478–2490
22. Gregory, C. W., He, B., Johnson, R. T., Ford, O. H., Mohler, J. L., French, F. S., and Wilson, E. M. (2001) *Cancer Res.* **61,** 4315–4319
23. Bai, S., He, B., and Wilson, E. M. (2005) *Mol. Cell. Biol.* **25,** 1238–1257
24. Tan, J. A., Sharief, Y., Hamil, K. G., Gregory, C. W., Zang, D. Y., Sar, M., Gumerlock, P. H., DeVere White, R. W., Pretlow, T. G., Harris, S. E., Wilson, E. M., Mohler, J. L., and French, F. S. (1997) *Mol. Endocrinol.* **11,** 450–459
25. Voegel, J. J., Heine, M. J., Tini, M., Vivat, V., Chambon, P., and Gronemeyer, H. (1998) *EMBO J.* **17,** 507–519
26. Huang, W., Shostak, Y., Tarr, P., Sawyers, C., and Carey, M. (1999) *J. Biol. Chem.* **274,** 25756–25768
27. Gregory, C. W., Johnson, R. T., Mohler, J. L., French, F. S., and Wilson, E. M. (2001) *Cancer Res.* **61,** 2892–2898
28. He, B., Bowen, N. T., Minges, J. T., and Wilson, E. M. (2001) *J. Biol. Chem.* **276,** 42293–42301
29. Lubahn, D. B., Joseph, D. R., Sar, M., Tan, J. A., Higgs, H. N., Larson, R. E., French, F. S., and Wilson, E. M. (1988) *Mol. Endocrinol.* **2,** 1265–1275
30. Stanley, T. B., Leesnitzer, L. M., Montana, V. G., Galardi, C. M., Lambert, M. H., Holt, J. A., Xu, H. E., Moore, L. B., Blanchard, S. G., and Stimmel, J. B. (2003) *Biochemistry* **42,** 9278–9287
31. Otwinowski, Z., and Minor, W. (1997) *Methods Enzymol.* **276,** 307–326
32. Vagin, A., and Teplyakov, A. (1997) *J. Appl. Crystallogr.* **30,** 1022–1025
33. Collaborative Computational Project Number 4 (1994) *Acta Crystallogr. Sect. D Biol. Crystallogr.* **50,** 760–763
34. Sack, J. S., Kish, K. F., Wang, C., Attar, R. M., Kiefer, S. E., An, Y., Wu, G. Y., Scheffler, J. E., Salvati, M. E., Krystek, S. R., Jr., Weinmann, R., and Einspahr, H. M. (2001) *Proc. Natl. Acad. Sci. U. S. A.* **98,** 4904–4909
35. Emsley, P., and Cowtan, K. (2004) *Acta Crystallogr. Sect. D Biol. Crystallogr.* **60,** 2126–2132
36. Murshudov, G. N., Vagin, A. A., and Dodson, E. J. (1997) *Acta Crystallogr. Sect. D Biol. Crystallogr.* **53,** 240–255
37. Lovell, S. C., Davis, I. W., Arendall, W. B., III, de Bakker, P. I. W., Word, J. M., Prisant, M. G., Richardson, J. S., and Richardson, D. C. (2003) *Protein Struct. Funct. Genet.* **50,** 437–450
38. Zhou, Z. X., Sar, M., Simental, J. A., Lane, M. V., and Wilson, E. M. (1994) *J. Biol. Chem.* **269,** 13115–13123
39. Wang, Q., Lu, J., and Yong, E. L. (2001) *J. Biol. Chem.* **276,** 7493–7499
40. Gregory, C. W., Fei, X., Ponguta, L. A., He, B., Bill, H. M., French, F. S., and Wilson, E. M. (2004) *J. Biol. Chem.* **279,** 7119–7130
41. Matias, P. M., Donner, P., Coelho, R., Thomaz, M., Peixoto, C., Macedo, S., Otto, N., Joschko, S., Scholz, P., Wegg, A., Basler, S., Schafer, M., Egner, U., and Carrondo, M. A. (2000) *J. Biol. Chem.* **275,** 26164–26171
42. Estebanez-Perpina, E., Moore, J. M., Mar, E., Delgado-Rodrigues, E., Nguyen, P., Baxter, J. D., Buehrer, B. M., Webb, P., Fletterick, R. J., and Guy, R. K. (2005) *J. Biol. Chem.* **280,** 8060–8068
43. Bohl, C. E., Miller, D. D., Chen, J., Bell, C. E., and Dalton, J. T. (2005) *J. Biol. Chem.* **280,** 37747–37754
44. Bohl, C. E., Gao, W., Miller, D. D., Bell, C. E., and Dalton, J. T. (2005) *Proc. Natl. Acad. Sci. U. S. A.* **102,** 6201–6206
45. Ostrowski, J., Kuhns, J. E., Lupisella, J. A., Manfredi, M. C., Beehler, B. C., Krystek, S. R., Bi, Y., Sun, C., Seethala, R., Golla, R., Sleph, P. G., Fura, A., An, Y., Kish, K. F., Sack, J. S., Mookhtiar, K. A., Grover, G. J., and Hamann, L. G. (2007) *Endocrinology* **148,** 4–12
46. Imperato-McGinley, J., Guerrero, L., Gautier, T., and Peterson, R. E. (1974) *Science* **186,** 1213–1215
47. Grino, P. B., Griffin, J. E., and Wilson, J. D. (1990) *Endocrinology* **126,** 1165–1172
48. Mahendroo, M. S., Cala, K. M., Hess, D. L., and Russell, D. W. (2001) *Endocrinology* **142,** 4652–4662
49. Maes, M., Sultan, C., Zerhouni, N., Rothwell, S. W., and Migeon, C. J. (1979) *J. Steroid Biochem.* **11,** 1385–1392
50. Shan, S. O., and Herschlag, D. (1996) *Proc. Natl. Acad. Sci. U. S. A.* **93,** 14474–14479
51. Pereira de Jesus-Tran, K., Cote, P. L., Cantin, L., Blanchet, J., Labrie, F., and Breton, R. (2006) *Protein Sci.* **15,** 987–999
52. Matias, P. M., Carrondo, M. A., Coelho, R., Thomaz, M., Zhao, X. Y., Wegg, A., Crusius, K., Egner, U., and Donner, P. (2002) *J. Med. Chem.* **45,** 1439–1446
53. Baker, E. N., and Hubbard, R. E. (1984) *Prog. Biophys. Mol. Biol.* **44,** 97–179
54. Holterhus, P. M., Sinnecker, G. H., and Hiort, O. (2000) *J. Clin. Endocrinol. Metab.* **85,** 3245–3250
55. Taplin, M. E., Bubley, G. J., Shuster, T. D., Frantz, M. E., Spooner, A. E., Ogata, G. K., Keer, H. N., and Balk, S. P. (1995) *N. Engl. J. Med.* **332,** 1393–1398
56. Duff, J., and McEwan, I. J. (2005) *Mol. Endocrinol.* **19,** 2943–2954
57. Kemppainen, J. A., Langley, E., Wong, C. I., Bobseine, K., Kelce, W. R., and Wilson, E. M. (1999) *Mol. Endocrinol.* **13,** 440–454
58. Zhou, Z. X., Lane, M. V., Kemppainen, J. A., French, F. S., and Wilson, E. M. (1995) *Mol. Endocrinol.* **9,** 208–218
59. Ong, Y. C., Kolatkar, P. R., and Yong, E. L. (2002) *Mol. Hum. Reprod.* **8,** 101–108
60. Shaneyfelt, T., Husein, R., Bubley, G., and Mantzoros, C. S. (2000) *J. Clin. Oncol.* **18,** 847–853
61. Gann, P. H., Hennekens, C. H., Ma, J., Longcope, C., and Stampfer, M. J. (1996) *J. Natl. Cancer Inst.* **88,** 1118–1126
62. Page, S. T., Lin, D. W., Mostaghel, E. A., Hess, D. L., True, L. D., Amory, J. K., Nelson, P. S., Matsumoto, A. M., and Bremner, W. J. (2006) *J. Clin. Endocrinol. Metab.* **91,** 3850–3856
63. Mohler, J. L., Gregory, C. W., Ford, O. H., Kim, D., Weaver, C. M., Petrusz, P., Wilson, E. M., and French, F. S. (2004) *Clin. Cancer Res.* **10,** 440–448
64. Sharrow, S. D., Edmonds, K. A., Goodman, M. A., Novotny, M. V., and Stone, M. J. (2005) *Protein Sci.* **14,** 249–256
65. Takano, K., Yamagata, Y., Kubota, M., Funahashi, J., Fujii, S., and Yutani, K. (1999) *Biochemistry* **38,** 6623–6629
66. Connelly, P. R., Aldape, R. A., Bruzzese, F. J., Chambers, S. P., Fitzgibbon, M. J., Fleming, M. A., Itoh, S., Livingston, D. J., Navia, M. A., Thomson, J. A., and Wilson, K. P. (1994) *Proc. Natl. Acad. Sci. U. S. A.* **91,** 1964–1968
67. Fischer, S., and Verma, C. S. (1999) *Proc. Natl. Acad. Sci. U. S. A.* **96,** 9613–9615